A NEW DETERMINATION OF THE HIGH-REDSHIFT TYPE Ia SUPERNOVA RATES WITH THE *HUBBLE SPACE TELESCOPE* ADVANCED CAMERA FOR SURVEYS[1]

N. Kuznetsova,[2,3] K. Barbary,[2,4] B. Connolly,[5] A. G. Kim,[2] R. Pain,[6] N. A. Roe,[2] G. Aldering,[2] R. Amanullah,[7] K. Dawson,[2] M. Doi,[8] V. Fadeyev,[9] A. S. Fruchter,[10] R. Gibbons,[11] G. Goldhaber,[2,4] A. Goobar,[12] A. Gude,[4] R. A. Knop,[11] M. Kowalski,[13] C. Lidman,[14] T. Morokuma,[15] J. Meyers,[2,4] S. Perlmutter,[2,4] D. Rubin,[2,4] D. J. Schlegel,[2] A. L. Spadafora,[2] V. Stanishev,[12] M. Strovink,[2,4] N. Suzuki,[2] L. Wang,[16] AND N. Yasuda[17]

(SUPERNOVA COSMOLOGY PROJECT)

Received 2007 May 1; accepted 2007 October 13

ABSTRACT

We present a new measurement of the volumetric rate of SNe Ia up to a redshift of 1.7, using the *HST* GOODS data combined with an additional *HST* data set covering the GOODS-North field collected in 2004. We employ a novel technique that does not require spectroscopic data for identifying SNe Ia (although spectroscopic measurements of redshifts are used for over half the sample); instead, we employ a Bayesian approach using only photometric data to calculate the probability that an object is an SN Ia. This Bayesian technique can easily be modified to incorporate improved priors on SN properties, and it is well-suited for future high-statistics SN searches in which spectroscopic follow-up of all candidates will be impractical. Here the method is validated on both ground- and space-based SN data having some spectroscopic follow-up. We combine our volumetric rate measurements with low-redshift SN data and fit to a number of possible models for the evolution of the SN Ia rate as a function of redshift. The data do not distinguish between a flat rate at redshift >0.5 and a previously proposed model, in which the Type Ia rate peaks at redshift ~1 due to a significant delay from star formation to the SN explosion. Except for the highest redshifts, where the signal-to-noise ratio is generally too low to apply this technique, this approach yields uncertainties that are smaller than or comparable to previous work.

Subject headings: supernovae: general

Online material: color figures

1. INTRODUCTION

The empirical evidence for the existence of dark energy came from observations of Type Ia supernovae (SNe Ia; Riess et al. 1998; Perlmutter et al. 1999; for review see Perlmutter & Schmidt 2003), which are believed to arise from the thermonuclear explosion of a progenitor white dwarf after it approaches the Chandrasekhar mass limit (Chandrasekhar 1931). However, the physics of SN Ia production is not well understood. The two most plausible scenarios for the white dwarf to accrete the necessary mass are the single-degenerate case, where the white dwarf is located in a binary system, and the double-degenerate case, where two white dwarfs merge. The SN Ia rate is correlated with the star formation history (SFH), and thus a measurement of the rate as a function of redshift helps constrain the possible Type Ia progenitor models.

In addition to its importance for understanding SNe Ia as astronomical objects, a good grasp of the SN Ia rate to high redshifts is important for the next generation of proposed space-based SN cosmology experiments, such as *SNAP* (Aldering et al. 2004). It is therefore of great practical interest to determine the rate of SNe Ia at redshifts >1.

The subject of SN Ia rates has been addressed by many authors in the past. Existing rate measurements have been mostly limited to redshift ranges <1: the results of Cappellaro et al. (1999), Hardin et al. (2000), Madgwick et al. (2003), and Blanc et al. (2004) measure the rates at redshifts ≲0.1; Neill et al. (2006), Tonry et al. (2003), and Pain et al. (2002) at intermediate redshifts of 0.47, 0.50, and 0.55, respectively; and Barris & Tonry (2006) up to a redshift of 0.75. Up until recently, the only published measurement of the rates at redshifts >1 has been that of Dahlen et al. (2004) who analyzed the GOODS data set. An analysis of the rates to redshift 1.6 has recently been completed using the Subaru Deep Field (Poznanski et al. 2007b).

There are several important differences that distinguish our work from that of Dahlen et al. (2004). First, we augment the GOODS sample with the *Hubble Space Telescope* (*HST*) data

[2] E. O. Lawrence Berkeley National Laboratory, Berkeley, CA 94720; nvkuznetsova@lbl.gov.

[3] Current address: Physics Department, Hamilton College, Clinton, NY 13323.

[4] Department of Physics, University of California, Berkeley, CA 94720.

[5] Department of Physics, Columbia University, New York, NY 10027.

[6] LPNHE, CNRS-IN2P3, University of Paris VI and VII, Paris, France.

[7] Space Sciences Laboratory, University of California, Berkeley, CA 94720.

[8] Institute of Astronomy, School of Science, University of Tokyo, Mitaka, Tokyo 181-0015, Japan.

[9] Department of Physics, University of California, Santa Cruz, CA 95064.

[10] Space Telescope Science Institute, Baltimore, MD 21218.

[11] Department of Physics and Astronomy, Vanderbilt University, Nashville, TN 37240.

[12] Department of Physics, Stockholm University, Albanova University Center, S-106 91 Stockholm, Sweden.

[13] Humboldt Universität Institut für Physik, Berlin 12489, Germany.

[14] European Southern Observatory, Vitacura, Casilla 19001, Santiago 19, Chile.

[15] Optical and Infrared Astronomy Division, National Astronomical Observatory of Japan, Mitaka, Tokyo 181-8588, Japan.

[16] Department of Physics, Texas A&M University, College Station, TX 77843.

[17] Institute for Cosmic Ray Research, University of Tokyo, Kashiwa 277 8582, Japan.
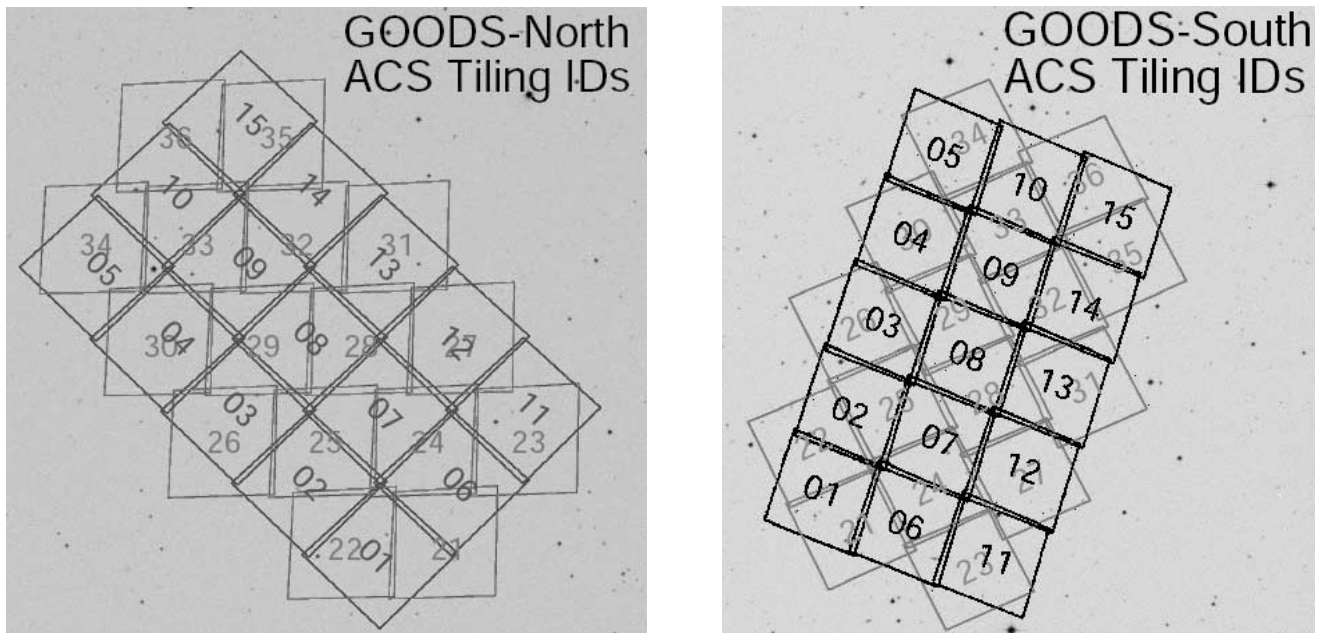
Fig. 1.—GOODS-N (*left*) and GOODS-S (*right*) fields. The fields are subdivided into tiles, which are shown (along with their ID numbers) in the panels. The size of a single tile is ∼11.5 arcmin². [*See the electronic edition of the Journal for a color version of this figure.*]

collected during the 2004 spring and summer high-redshift SN searches. Second, our methods of calculating the control time (the time during which an SN search is potentially capable of finding SN candidates) and the efficiency to identify an SN are based on a detailed Monte Carlo simulation technique using a library of SN templates. Third, we adopt a novel approach to typing SNe, using photometric data and a Bayesian probability method described in Kuznetsova & Connolly (2007). The Bayesian technique is able to perform classification using only photometric data and therefore does not require spectroscopic follow-up. Optionally, photometric or spectroscopic redshifts can be used to improve the classification accuracy. Our initial requirements on potential SN candidates are more stringent in terms of the number of points on the light curve and the signal-to-noise ratio (S/N) of those points than those of Dahlen et al. (2004); thus, some of the candidates they identified will fail our cuts. However, we are able to reliably separate SNe Ia from other SN types based on their Bayesian probability, with an efficiency that is readily quantifiable, thus allowing us to use larger data samples. Our approach therefore avoids the problems that arise in estimating the efficiency for the decision to schedule spectroscopic follow-up based on a potentially low S/N initial detection.

The Bayesian classification technique uses photometric data and does not require any spectroscopic follow-up. This is an advantage for future large-area surveys (such as the Dark Energy Survey, Pan-STARRS, and LSST) that will discover thousands of SN candidates but are unlikely to be able to obtain spectroscopic data for all of them, to distinguish SNe Ia from core-collapse (CC) SNe and other variable objects. The technique described here can be considered a prototype of the kind of analysis that could be performed on these future large data sets to identify SNe Ia for cosmological studies. There is a clear trade-off involved in using photometric measurements alone: if the quality of the photometric data is poor, then the efficiency of this technique to identify SNe Ia is reduced; on the other hand, this technique enables larger samples of Type Ia from imaging surveys to be identified for cosmological studies, without the need for time-consuming spectroscopic follow-up.

Note that although the method is able to perform the SN typing with photometric data alone (i.e., it does not require spectroscopic data, either redshifts or types), it is certainly able to use the extra information that is available, and in fact 70% of the SN candidates discussed in the present work have redshifts that were obtained spectroscopically. It is also worth noting that while in this paper we only analyze the SN Ia rates, the Bayesian classification technique can be used to classify other types as well, making it possible to measure the rates of non–Type Ia SNe in a similar fashion. These analyses will be presented in future publications.

The paper is organized as follows. In § 2 we describe the data samples used in the analysis. In § 3 we describe the SN candidate selection and typing process. In § 4 we calculate the control time, survey area, and search efficiency and determine the volumetric SN Ia rate from our data sample. A comparison of the rates with those reported in the literature is given in § 5, and fits of the rates to different models relating the SN Ia rates to the SFH are given in § 6. A summary is given in § 7.

2. DATA SAMPLE

For this analysis, we use the *HST* GOODS data set collected in 2002–2003 (Renzini et al. 2003; Dickinson et al. 2003; Giavalisco et al. 2004). In addition to the GOODS data, we use an *HST* sample collected in the spring and summer of 2004, which we hereafter call the 2004 Advanced Camera for Surveys (ACS) sample. The GOODS data set consists of five epochs (data taking periods), separated by approximately 45 observer-frame days. The GOODS data used for this analysis were taken in two *HST* ACS filter bands: F775W (centered at 775 nm) and F850LP (centered at 850 nm).[18] Each F850LP image consists of four exposures, and each F775W image consists of two exposures. The GOODS survey includes two fields, GOODS-North (GOODS-N) and GOODS-South (GOODS-S), and covers

---

[18] The ACS filter transmission curves are available at http://acs.pha.jhu.edu/instrument/filters.

TABLE 1
Summary of the Data Sets Used in This Analysis

Epoch	Filter	Exposure Time (s)	Filter	Exposure Time (s)	Number of Tiles	Taken on
GOODS-S						
1.......................................	F775W	1040	F850LP	2120	15	2002 Jul 31–Aug 4
2.......................................	F775W	1040	F850LP	2120	16	2002 Sep 19–22
3.......................................	F775W	1040	F850LP	2120	15	2002 Oct 31–Nov 3
4.......................................	F775W	1040	F850LP	2120	16	2002 Dec 19–22
5.......................................	F775W	1040	F850LP	2120	15	2003 Feb 1–5
GOODS-N						
1.......................................	F775W	1120	F850LP	2400	14	2002 Nov 21–22
2.......................................	F775W	1000[a]	F850LP	2120	17	2003 Jan 2–4
3.......................................	F775W	960	F850LP	2060	16	2003 Feb 20–23
4.......................................	F775W	960	F850LP	2000	14	2003 Apr 3–6
5.......................................	F775W	960	F850LP	2080	15	2003 May 21–25
2004 ACS Sample (GOODS-N Tiles)						
1.......................................	F775W	400	F850LP	1600	15	2004 Apr 2–4
2.......................................	F775W	400	F850LP	1600	15	2004 May 20–23
3.......................................	F775W	400	F850LP	1600	15	2004 Jul 9–10
4.......................................	F775W	400	F850LP	1600	15	2004 Aug 26–28

Note.—A summary of the data sets used in this analysis, listing the data taking epochs, the filters, the exposure times of the combined exposures (in seconds), the number of GOODS field tiles, and the dates when the data were taken.

[a] Except for tile 30 (1060).

approximately 320 arcmin². The fields are subdivided into smaller "tiles" that correspond to single ACS pointings (typically 15 or 16), as shown in Figure 1.

The 2004 ACS SN data set covers only the GOODS-N field, with the same tiling as that of the GOODS-N data set. It consists of four epochs separated by approximately 45 observer-frame days. The data in this sample were taken in two *HST* ACS passbands: F775W and F850LP, with one exposure for every F775W image and four for every F850LP image. Two teams (PI Perlmutter and PI Riess) shared this data searching for SNe in alternate visits; Riess et al. (2007) have published the results for the SNe that were discovered in their team's visits.

For convenience, a summary of the data sets used is given in Table 1.

It is worth emphasizing that we are using photometric information from only two filter bands, providing one color measurement. The GOODS data set has been analyzed before, and 13 out of 42 SNe found were spectroscopically typed (Riess et al. 2004b; Strolger et al. 2004). For the 2004 ACS sample, however, the spectroscopic information is available only for a small fraction of the candidates. We treat both GOODS and 2004 ACS data sets in a consistent fashion, using photometric information only for typing SNe (note that we still use spectroscopically determined redshifts where available). This allows more data to be searched and more SNe to be found, but at the expense of neglecting spectroscopic information for the candidates where it is available. In § 3.3 we discuss in detail the resulting SN candidate count.

We start with the data that have been flat-fielded and gain-corrected by the *HST* pipeline and use MultiDrizzle (Fruchter & Hook 2002) to perform cosmic-ray rejection and to combine dithered observations. The parameters of the drizzling process include a "square" kernel, with a pixel fraction of 0.66 and a pixel scale of 1.0. The drizzling combines the multiple individ-

ual pointings. Drizzling is ineffective for the cosmic-ray rejection for the F775W data from the 2004 ACS sample since they contain only a single exposure for each GOODS-N tile. We therefore use a morphological cosmic-ray rejection package (van Dokkum 2001) to create images with identifiable objects, thus allowing us to generate the geometrical transformations between images; however, the original images are used for extracting photometric information (after verifying that no cosmic rays landed directly at the location of the SN candidates).

SNe are identified by subtracting a reference image from each of the *HST* search epochs. We create four distinct samples summarized in Table 2, which we use for identifying and performing simple aperture photometry on the SN candidates in each of the five epochs in the GOODS data set and each of the four epochs in the 2004 ACS data set. To obtain the multiepoch photometry for the GOODS-N data (sample 1), we combine all four epochs of the 2004 ACS sample and then subtract these data from each of the five GOODS-N epochs in turn. Combining multiple epochs for the reference image allows us to create deeper resulting data, which is important for extracting SNe with the best possible S/N. For sample 2, we combine the entire GOODS-N sample and subtract these data from each of the four 2004 ACS epochs in turn. Because the GOODS and 2004 ACS data were taken with a time separation of approximately 1 yr, these samples should be sensitive to the SNe that were both on the rise and on the decline during the GOODS and 2004 ACS data-taking period for samples 1 and 2, respectively. For the GOODS-S sample, however, we do not have any additional data sets and are thus forced to separate the sample into two. This is the reason the three initial data samples (GOODS-N and GOODS-S and the 2004 ACS data set) result in four search samples. We combine GOODS-S epochs 4 and 5 for sample 3, and epochs 1 and 2 for sample 4; we then subtract the two combined samples separately from each of the five GOODS-S epochs.

TABLE 2
Samples Used in Our Supernova Search

Sample (1)	Reference Data Set (2)	Supernova Search (3)
1...	Combined 2004 ACS data (four epochs)	Individual GOODS-N epochs
2...	Combined GOODS-N data (five epochs)	Individual 2004 ACS data set epochs
3...	Epochs 4+5 of the GOODS-S data	Individual GOODS-S epochs
4...	Epochs 1+2 of the GOODS-S data	Individual GOODS-S epochs

Notes.—To identify and extract photometry for SN candidates, we subtract the data listed in col. (2) from the data listed in col. (3). Note that sample 2 has the deepest references.

If an SN candidate has been found in both samples 3 and 4, we consider it to belong to the sample in which it had an epoch with the largest S/N. This avoids any possible double counting of the candidates for the GOODS-S data.

3. THE SUPERNOVA CANDIDATE SELECTION AND TYPING

The search for SN candidates and their subsequent typing as SNe Ia is a three-stage process. We briefly describe them below, and then in detail in §§ 3.1–3.3:

1. First, potential SN candidates in individual epochs are identified by the software that is used to subtract the SN search data from the reference data. The initial candidate selection is done using the F850LP data only because it suffers less from cosmic-ray contamination and because F850LP covers SNe at redshifts up to ∼1.5. The initial SN selection is primarily directed toward reducing the number of false positives resulting from various image processing artifacts and residual cosmic-ray contamination. It is followed by a manual scan to reject any obvious remaining cosmic rays and image processing artifacts. Note that both sources of false detections have specific signatures that real SNe do not have; this selection therefore is not expected to reduce the number of real SNe in the sample. This stage is described in detail in § 3.1.

2. For the candidates on individual epochs that pass the first stage of the selection process, we extract the photometric information at the candidate locations in the multiepoch F850LP and F775W data. We then select candidates with reasonably well measured light curves by requiring that the candidate's S/N in the subtracted data (in both filters) be greater than 2 for at least three search epochs, including at least two with an S/N greater than 3. At the end of this stage, we are left with the majority of candidates that are presumed to be SNe of some type, as well as some candidates that cannot be modeled as any known SN type. This stage is described in detail in § 3.2.

3. The final step applies a Bayesian likelihood technique that assigns each candidate that passed steps 1 and 2 a probability to be an SN Ia based on the multiepoch data in both filters. This stage is described in detail in § 3.3.

For convenience, we summarize the selection process in Table 3. We now describe each of the selection stages in detail.

3.1. Stage 1: Single-Epoch Supernova Candidate Selection

In the first step of the SN search, we search for SN candidates in the individual epochs of the F850LP data by looking for signals in the reference-subtracted search images. The reference image is the same for each exposure (recall that each F850LP image consists of four exposures, each with the same exposure time). We use aperture photometry with a radius of 3 pixels, where the pixel scale is $0.03''$ (after drizzling). This choice of the aperture optimizes the S/N of SN candidates. We verified that the photometric extraction procedure is working well by creating "fake" SNe, as described later in this section, and comparing their input and output magnitudes; they agree at the subpercent level. The procedure for identifying SNe is as follows:

1. Subtracting the combined (drizzled) exposures of the search data from the (drizzled) reference data, we require the following:

a) The absolute value of the flux within the SN candidate's aperture in the subtracted data divided by the flux in the reference data (the "percent increase" variable) must be ≥15%.
b) The candidate's shape in the subtracted data must be consistent with a point source: we require that the candidate's FWHM in both *x*- and *y*-directions be <4 pixels and that the absolute value of its normalized *xy* moment be <0.5 pixels.

2. Next, to eliminate false detections resulting from cosmic rays, we do the following:

a) We consider the four individual exposures of the search images. The S/N measured for an SN candidate in each of these exposures ($S/N_{exposure}$) should be at least 3. A false positive resulting from cosmic rays will likely not be present in every individual exposure.

TABLE 3
Summary of the SN Ia Selection and Typing Process

Selection Stage	Data Used	Cuts Applied
1...	F850LP, single (discovery) epoch	$S/N_{exposure} > 3$ in four exposures; S/N consistency in three out of four exposures; percent increase ≥15% in combined exposures; shape cuts in combined exposures
2...	F850LP, F775W, all epochs	≥3 epochs with S/N > 2 (including ≥2 epochs with S/N > 3)
3...	F850LP, F775W, all epochs	Bayesian Type Ia classification

Note.—The meaning of the cuts is explained in the text describing the corresponding stages.
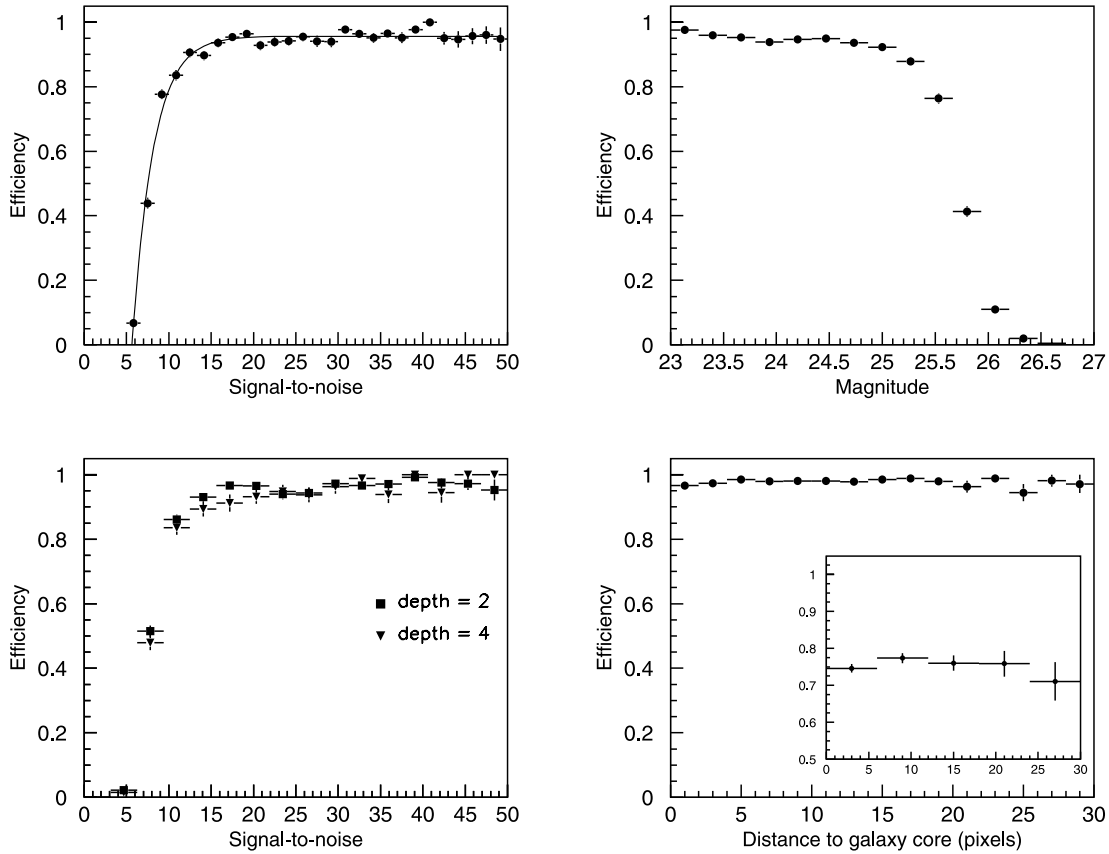
Fig. 2.— Efficiency of the stage 1 SN selection in the reference-subtracted search images. The errors are assigned using binomial statistics. *Top left*: Combined efficiency for all depths (see text for the definition of depth) of the reference image as a function of the candidate's S/N. Overlaid as a solid line is the fit of the efficiency to the function in eq. (1). *Top right*: Same as the top left panel, but as a function of the candidates' magnitude. *Bottom left*: Efficiencies for two representative depths: 2 (*squares*) and 4 (*triangles*). *Bottom right*: Efficiency as a function of the SN distance from the host galaxy core for all candidates with S/N > 15; the insert shows the efficiency for the candidates with S/N ≤ 15. [*See the electronic edition of the Journal for a color version of this figure.*]

b) We then subtract each of the individual exposures from the reference image at the location of the SN candidate and compare the signal to the quadratic sum of the noise. The difference in these S/Ns between the exposures must be <3 for at least three out of four exposures. We are thus allowing one (and only one) of the four exposures of the search image to be contaminated by a cosmic ray.

These cuts eliminate close to 90% of false detections (i.e., the number of detections decreases from ∼100 per single tile [see Fig. 1] to ∼10). Obvious image processing artifacts or cosmic rays that manage to pass these cuts are rejected by manual screening (typically, there would be a few such candidates per tile, mostly image processing artifacts), with any questionable candidates left in the sample. The efficiency of the manual scan has been checked using a sample of ∼100 fake SNe, generated as described below, and 100% were correctly identified. The preliminary selection flags any variable objects: SNe of various types, as well as active galactic nuclei (AGNs), etc. In § 3.3 we describe our approach to selecting SNe Ia from the sample.

In order to measure the efficiency of the selection, we used a Monte Carlo simulation that puts fake SNe on real F850LP images. Fake SNe were also used to develop the selection cuts listed above in an unbiased way. The technique follows the approach outlined in Pain et al. (1996) and works as follows.

First, we run SExtractor (Bertin & Arnouts 1996) version 2.3 on the search images that have been combined, or drizzled, together from the individual exposures. We do this for a number of both GOODS-N and GOODS-S tiles. Using SExtractor's classi-

fication of objects as galaxies and stars, we create a list of the galaxy positions on the image. Because in our analysis we are ignoring candidates near image edges, the galaxies located within two galaxy FWHMs (also determined by SExtractor) from the image boundaries are discarded. The fake SN that is to be put on the image is randomly assigned a magnitude that is drawn from a flat distribution between 23 and 30. The SN's position is drawn from a Gaussian distribution with half the galaxy's FWHM as the standard deviation and centered on the galaxy's nominal center. We then use the STSDAS[19] `tranback` function to convert the fake SN positions on the drizzled images into coordinates on the raw individual exposures. Fake SNe themselves are created using the Tiny Tim software (Krist & Hook 2004, p. 339), for the ACS WFC1 camera, in filter F850LP. The fake SN signal, combined with a noise generated using a Poisson distribution with the signal's mean for each pixel, is added onto the input exposures, which are subsequently processed in exactly the same way as real data are.

We generated ∼13,000 fake SNe (the 100 SNe used for the check of the manual scanning efficiency were a subset of this sample). The fake SNe that pass the stage 1 selection cuts described above are compared with the input list of fakes. This allows us to calculate the efficiency of the selection cuts for the preliminary SN selection. This efficiency is shown in the top left panel of Figure 2 as a function of the candidates' S/N and in the

---

TABLE 4
Candidates Selected at the End of Stage 2 for Sample 1

Candidate	R.A. (J2000.0)	Decl. (J2000.0)	Redshift	Error	Source	Reference	Comment	$P(\mathrm{Ia}|\{D_i\}, z)$
1........................	12 37 06.938	+62 09 15.81	0.53	0.25	host phot	1		1.0
2........................	12 37 01.537	+62 11 28.66	0.778	0.001	host spec	2		1.0
3........................	12 36 56.336	+62 11 55.65	0.83	0.10	host phot	1		1.0
4........................	12 37 49.350	+62 14 05.71	0.41	0.01	spec	3	Silver CC (SN 2002kl)	0.3
5........................	12 36 21.291	+62 11 01.24	0.633	0.001	host spec	4		0.9
6........................	12 37 08.396	+62 14 23.98	0.564	0.001	host spec	4		0.9
7........................	12 37 40.658	+62 20 07.42	0.741	0.001	host spec	4		1.0
8........................	12 36 16.850	+62 14 37.30	0.71	0.05	host phot	3	Bronze Ia (SN 2002kh)	1.0
9........................	12 37 28.421	+62 20 39.56	1.141	0.001	(host+SN) spec	5	Gold Ia (SN 2002ki)	1.0
10........................	12 36 38.130	+62 09 52.88	0.513	0.001	host spec	3, 4	Silver CC (SN 2003bc)	0.0
11........................	12 37 25.126	+62 13 16.98	0.67	0.01	SN spec	5	Gold Ia (SN 2003bd)	1.0
12........................	12 36 24.506	+62 08 34.84	0.954	0.001	host spec	3, 4	Silver CC (SN 2003bb)	0.8
13........................	12 36 27.828	+62 11 24.71	0.66	0.05	host phot	3	Bronze CC (SN 2003ew)	1.0
14........................	12 37 19.723	+62 18 37.23	1.27	0.01	SN spec	5	Gold Ia (SN 2003az)	1.0
15........................	12 37 15.208	+62 13 33.55	0.899	0.001	(host+SN) spec	4, 5	Gold Ia (SN 2003eb)	0.0
16........................	12 36 55.441	+62 13 11.46	0.954	0.001	(host+SN) spec	4, 5	Gold Ia (SN 2003es)	1.0
17........................	12 36 33.179	+62 13 47.34	0.54	0.05	host phot	3	Bronze Ia (SN 2003en)	0.9
18........................	12 36 57.900	+62 17 23.24	0.529	0.001	host spec	4		1.0
19........................	12 36 39.967	+62 07 52.12	0.48	0.05	host phot	3	Bronze CC (SN 2003dz)	0.9
20........................	12 36 31.772	+62 08 48.25	0.46	0.05	host phot	3	Bronze CC (SN 2003dx)	0.0
21........................	12 37 28.992	+62 11 27.36	0.935	0.001	host spec	3, 4	Silver Ia (SN 2003lv)	N/A
22........................	12 37 09.189	+62 11 28.17	1.340	0.001	(host+SN) spec	4, 5	Gold Ia (SN 2003dy)	1.0
23........................	12 37 12.066	+62 12 38.04	0.89	0.05	host phot	3	Bronze CC (SN 2003ea)	0.4
24........................	12 36 15.925	+62 12 37.38	0.286	0.001	host spec	3, 4	Bronze CC (SN 2003ba)	N/A
25........................	12 36 26.718	+62 06 15.16	0.618	0.001	host spec	6		N/A
26........................	12 36 26.013	+62 06 55.11	0.638	0.001	(host+SN) spec	4, 5	Gold Ia (SN 2003be)	1.0

Notes.—Listed are the candidates' coordinates, redshifts, errors on the redshifts, the sources used for the redshift and redshift error determination, the references for the sources, and $P(\mathrm{Ia}|\{D_i\}, z)$ defined in § 3.3 (the "N/A" stands for a special category of candidates designated as "anomalies," as described in § 3.3). Units of right ascension are hours, minutes, and seconds, and units of declination are degrees, arcminutes, and arcseconds. For the candidates found in Riess et al. (2004b) the tables also list the SN name and classification (gold, silver, or bronze).

References.— (1) B. Mobasher & T. Dahlen 2004, private communication; (2) Cowie et al. 2004; (3) Strolger et al. 2004; (4) Wirth et al. 2004; (5) Riess et al. 2004b; (6) this paper.

top right panel of Figure 2 as a function of the candidates' magnitude, on the reference-subtracted search images. Note that our reference images are not uniformly deep: they consist of two, four, or five combined epochs, depending on the tile of the GOODS field and the SN's position on the tile (see Fig. 1). The bottom left panel of Figure 2 shows the SN finding efficiency as a function of the S/N for two representative cases: (1) for all locations where two epochs contribute to the reference data, and (2) for all locations where there are four epochs that are available for the reference data. We refer to these cases as "depth 2" and "depth 4," respectively. It is evident that, within errors, for a given S/N, the efficiency is independent of the depth of the reference image at the location of the fake SNe, as it should be. We thus use the efficiency curve in Figure 2 (*top left panel*) that combines all of the depths, which we fit to the following four-parameter function:

$$\epsilon(\mathrm{S/N}) = p_1 + \frac{p_2}{1 + e^{p_3(\mathrm{S/N} - p_4)}}, \qquad (1)$$

where we obtain $p_1 = 0.96$, $p_2 = -18.04$, $p_3 = 0.41$, and $p_4 = -1.34$. The resulting fit is also shown in Figure 2 (*top left panel*).

One concern in SN searches is the potential loss of candidates located close to the core of their host galaxies. The bottom right panel of Figure 2 shows the efficiency as a function of the SN's distance from the galaxy core. It is apparent that the efficiency remains essentially flat.

3.2. *Stage 2: The Multiepoch Selection*

The second stage of the SN candidate selection is where we turn to the multiepoch photometric data in both filters. Subtracting the stacked image of each epoch of the search data from the reference data, we calculate the candidates' S/Ns in the subtracted data and require that there be at least three epochs with S/N > 2, including at least two epochs with S/N > 3. These cuts are designed to select candidates with reasonably well measured light curves. Because the Bayesian technique described in § 3.3 provides a powerful discrimination of SNe Ia, these cuts can be very loose. At the end of stage 2, we have 26 candidates in sample 1, 17 candidates in sample 2, 9 candidates in sample 3, and 5 candidates in sample 4, for a total of 57 candidates. A list of these candidates is given in Tables 4, 5, 6, and 7, for samples 1, 2, 3, and 4, respectively. The tables specify the SN names and classifications (gold, silver, or bronze) for the candidates that were also found in Riess et al. (2004b, 2007). The classification refers to the degree of belief in the typing of the candidate, with gold being certain. For sample 1, we have eight gold SNe Ia, one silver SN Ia, and three silver CC SNe. For samples 3 and 4, we have five gold and two silver SNe Ia, and one gold and one silver CC SN. There were six additional gold and silver SNe Ia found in Riess et al. (2004b) that failed our stage 2 cuts (SN 2003eu, SN 2002lg, SN 2002fx, SN 2003ak, SN 2003eq, and SN 2003al) because they did not have a sufficient number of epochs with high enough S/N. In other words, these candidates fall below the threshold that is intentionally set high enough that an automated

TABLE 5

Candidates Selected at the End of Stage 2 for Sample 2

Candidate	R.A. (J2000.0)	Decl. (J2000.0)	Redshift	Error	Source	Reference	Comment	$P(\mathrm{Ia}|\{D_i\}, z)$
1...............	12 36 20.889	+62 10 19.24	1.10	0.28	host phot	1		1.0
2...............	12 36 29.474	+62 11 41.40	1.35	0.40	host phot	1		0.0
3...............	12 36 19.901	+62 13 47.67	0.535	0.001	host spec	2		0.0
4...............	12 36 27.131	+62 15 09.27	0.794	0.001	host spec	2		0.0
5...............	12 36 32.238	+62 16 58.38	0.437	0.001	host spec	2		0.4
6...............	12 38 03.689	+62 17 12.23	0.280	0.001	host spec	3		0.4
7...............	12 37 09.495	+62 22 15.37	1.61	0.34	host phot	1		1.0
8...............	12 37 06.772	+62 21 17.46	0.406	0.001	host spec	2		0.1
9...............	12 36 26.694	+62 08 29.74	0.555	0.001	host spec	2		0.8
10.............	12 36 54.125	+62 08 22.21	1.39	0.01	SN spec	4	Gold Ia (HST04Sas)	1.0
11.............	12 36 34.363	+62 12 12.55	0.457	0.001	(host+SN) spec	2, 4	Gold Ia (JST04Yow)	1.0
12.............	12 37 33.918	+62 19 21.75	0.88	0.38	host phot	1		1.0
13.............	12 36 34.853	+62 15 48.86	0.855	0.001	(host+SN) spec	2, 4	Gold Ia (HST04Man)	1.0
14.............	12 36 36.009	+62 17 31.97	0.60	0.15	host phot	1		0.2
15.............	12 36 55.214	+62 13 03.75	0.952	0.004	(host+SN) spec	4, 5	Gold Ia (HST04Tha)	1.0
16.............	12 37 48.435	+62 13 34.85	0.839	0.001	host spec	2		1.0
17.............	12 36 01.542	+62 15 55.16	0.086	0.001	host spec	6		N/A

Notes.—Units of right ascension are hours, minutes, and seconds, and units of declination are degrees, arcminutes, and arcseconds. The redshift of candidate 17 is uncertain, as the possible host galaxy is 7″ away. Leaving this redshift as unconstrained does not change our results.

References.—(1) B. Mobasher & T. Dahlen 2004, private communication; (2) Wirth et al. 2004; (3) Cowie et al. 2004; (4) Riess et al. 2007; (5) Cohen et al. 2000; (6) Hornschemeier et al. 2003.

Bayesian classification of candidates (discussed in § 3.3) may be possible. Note also that the failure of real SNe Ia to pass stage 2 cuts is taken into account in the control time calculation (§ 4.1).

Spectroscopic redshifts (of the host, the SN, or both) were taken from the following sources: Strolger et al. (2004), Riess et al. (2004b, 2007), Cohen et al. (2000), Cowie et al. (2004), Wirth et al. (2004), Le Fèvre et al. (2004), and Vanzella et al. (2006). In some cases, the spectroscopic redshift has been determined more than once. We find good agreement in such cases. If a spectroscopic redshift was not available, we used photometric redshifts from Wolf et al. (2004), Strolger et al. (2004), and B. Mobasher & T. Dahlen (2004, private communication).

The host galaxies of three candidates (candidates 9 and 25 in Table 4 and candidate 12 in Table 5) were observed with the Subaru Faint Object Camera and Spectrograph (FOCAS; Kashikawa et al. 2002) on 2007 May 17. All three host galaxies were observed with the 300R grism and the SO58 order sorting filter, resulting in spectra covering the 5800–10000 Å spectral region with a resolving power of ~300. Single emission lines were

detected in the first two galaxies. If these lines are due to the [O ii] doublet at 3727 Å, then the redshifts of these sources are $z = 1.143 \pm 0.001$ and 0.618 ± 0.001, respectively. The first measurement confirms the redshift reported in Strolger et al. (2004). The second measurement is new. Although the continuum of the third galaxy was detected, no clear spectral features are apparent, so we used the photometric redshift instead.

The typical error in the redshift that is measured spectroscopically is 0.001, if the redshift was determined from host galaxy lines, or 0.01, if the redshift was determined from SN features. For photometric redshifts, the error is larger, ranging from 0.05 to as high as 0.4. The source of the redshift errors is listed in the tables as well. Precision photometric measurements for previously unpublished candidates will be made available in N. Suzuki et al. (2008, in preparation).

Note that the redshifts of candidate 17 in Table 5 and candidate 4 in Table 6 are uncertain, since the assumed host galaxies of the SN candidates are 7″ and 4″ away, respectively. However, we have verified that if we leave the redshifts of these candidates as unconstrained, it does not affect our final results.

TABLE 6

Candidates Selected at the End of Stage 2 for Sample 3

Candidate	R.A. (J2000.0)	Decl. (J2000.0)	Redshift	Error	Source	Reference	Comment	$P(\mathrm{Ia}|\{D_i\}, z)$
1..................	03 32 18.072	−27 41 55.83	0.88	0.05	host phot	1	Silver Ia (SN 2002fy)	0.9
2..................	03 32 13.002	−27 42 05.75	0.421	0.001	host spec	2		0.0
3..................	03 32 37.511	−27 46 46.40	1.30	0.01	SN spect	3	Gold Ia (SN 2002fw)	1.0
4..................	03 32 05.060	−27 47 02.96	0.976	0.001	host spec	2		N/A
5..................	03 32 17.309	−27 46 23.74	0.13	0.01	phot	4		0.0
6..................	03 32 48.598	−27 54 17.14	0.841	0.001	host spec	1, 2	Silver CC (SN 2002fz)	0.9
7..................	03 32 22.751	−27 51 09.65	Unconstrained	Unconstrained	phot	1	Bronze CC (SN 2002fv)	0.0
8..................	03 32 42.441	−27 50 25.08	0.58	0.01	spec	1	Gold CC (SN 2002kb)	N/A
9..................	03 32 38.082	−27 53 48.15	0.987	0.001	host spec	1, 2	Bronze Ia (SN 2002ga)	1.0

Notes.—Units of right ascension are hours, minutes, and seconds, and units of declination are degrees, arcminutes, and arcseconds. The redshift of candidate 4 is uncertain, as the possible host galaxy is 4″ away. Leaving this redshift as unconstrained does not change our results.

References.—(1) Strolger et al. 2004; (2) Le Fèvre et al. 2004; (3) Riess et al. 2004b; (4) Wolf et al. 2004.

TABLE 7
Candidates Selected at the End of Stage 2 for Sample 4

Candidate	R.A. (J2000.0)	Decl. (J2000.0)	Redshift	Error	Source	Reference	Comment	$P(\mathrm{Ia}|\{D_i\}, z)$
1........................	03 32 24.782	−27 46 18.07	1.306	0.001	host spec	1, 2	Gold Ia (SN 2002hp)	1.0
2........................	03 32 22.522	−27 41 52.26	0.526	0.001	(host+SN) spec	1	Gold Ia (SN 2002hr)	1.0
3........................	03 32 22.318	−27 44 27.04	0.738	0.001	host spec	1, 2	Gold Ia (SN 2002kd)	1.0
4........................	03 32 05.382	−27 44 29.76	0.91	0.05	host phot	3	Silver Ia (SN 2003al)	1.0
5........................	03 32 34.648	−27 39 58.18	0.214	0.001	(host+SN) spec	1, 4	Gold Ia (SN 2002kc)	1.0

Note.—Units of right ascension are hours, minutes, and seconds, and units of declination are degrees, arcminutes, and arcseconds.
References.—(1) Riess et al. 2004b; (2) Vanzella et al. 2006; (3) Strolger et al. 2004; (4) Le Fèvre et al. 2004.

3.3. *Stage 3: The Identification of Type Ia Supernovae*

The candidates that have been selected in stages 1 and 2 are assumed to be real transient objects, most likely SNe, and must now be classified by type. With only scarce photometric data available, we turn to the Bayesian method of classifying SNe described in Kuznetsova & Connolly (2007).

Photometric typing of SNe has been described in Poznanski et al. (2002), Riess et al. (2004a), Johnson & Crotts (2006), and Sullivan et al. (2006a), among others. Most of the existing methods rely on color-color or color-magnitude diagrams for SN classification, although a Bayesian approach similar to ours has recently been independently developed by Poznanski et al. (2007a).

In our method, we consider five possible SN types ("normal" Ia [Branch et al. 1993], Ibc, IIL, IIP, and IIn). We make use of the best currently available SN multicolor light-curve templates for each type. When improved SN templates are available, they can be easily worked into the method. We calculate the probability that a given SN candidate with photometric data $\{D_i\}$, where i is the index for the number of observational epochs, and redshift z is an SN Ia. By virtue of Bayes' theorem, this probability is given by

$$P(\mathrm{Ia}|\{D_i\}, z) = \frac{\int_{\boldsymbol{\theta}} P(\{D_i\}, z|\boldsymbol{\theta}, \mathrm{Ia}) P(\boldsymbol{\theta}, \mathrm{Ia}) \, d\boldsymbol{\theta}}{\sum_T \int_{\boldsymbol{\theta}} P(\{D_i\}, z|\boldsymbol{\theta}, T) P(\boldsymbol{\theta}, T) \, d\boldsymbol{\theta}}, \quad (2)$$

where z is the measured SN redshift; $\boldsymbol{\theta}$ are the parameters that characterize a given SN type, $\{D_i\}$ are the data in both F850LP and F775W, $P(\{D_i\}, z|\boldsymbol{\theta}, T)$ is the probability density to obtain data $\{D_i\}$ and redshift z for SN type T, $P(\boldsymbol{\theta}, T)$ contains prior information about type T SNe, and the denominator contains the normalization (the sum) over all five SN types T considered. The parameters $\boldsymbol{\theta} \equiv (\bar{z}, t_{\mathrm{diff}}, s, M, R_V, A_V)$ are as follows: $\bar{z}$ is the true SN redshift; t_{diff} is the time difference between the dates of maximum light for the template and the data; s is the stretch parameter (Perlmutter et al. 1997), which parameterizes the width of the light curve (if $T = \mathrm{Ia}$); M is the absolute magnitude in the rest-frame B band at maximum light; and A_V and R_V are the Cardelli-Clayton-Mathis interstellar extinction parameters (Cardelli et al. 1988). We marginalize (integrate over) these parameters as described below.

Suppose that we have a photometric template, $\{\bar{D}(\boldsymbol{\theta}, T)_i\}$, for the expected light curve for an SN of type T at a given redshift, $\bar{z}$. In this work, we use the templates from P. E. Nugent,[20] which extend both into the UV (below 3460 Å in the SN rest frame) and into far-red and IR (above 6600 Å in the SN rest frame) regions. It is assumed that the measured light-curve flux, $\{D_i\}$, can fluctuate from the template $\{\bar{D}(\boldsymbol{\theta}, T)_i\}$ according to Gaussian statistics. It is also assumed that the probability of

measuring redshift z fluctuates around a mean $\bar{z}$ according to Gaussian statistics as well. Therefore,

$$P(\{D_i\}, z|\boldsymbol{\theta}, T) = \frac{\exp\left[-(z - \bar{z})^2/2\delta z^2\right]}{\sqrt{2\pi}\delta z} \times \prod_{i=1}^{n_{\mathrm{epochs}}} \frac{\exp\left\{-\left[\bar{D}(\boldsymbol{\theta}, T)_i - D_i\right]^2/2\delta D_i^2\right\}}{\sqrt{2\pi}\delta D_i}, \quad (3)$$

where δD_i are photometric measurement errors for epoch i and δz is the measurement error for the redshift z. Note that we assume no errors on the SN templates themselves; we take them to represent the best currently available knowledge of the SN behavior. However, it is also worth noting that various parameters that characterize a given template (e.g., the peak rest-frame B-band magnitude, the stretch parameter for SNe Ia, etc.) are varied as described below, thus effectively representing some template variations.

The prior $P(\boldsymbol{\theta}, T)$ contains all the available information about the behavior of type T SNe, expressed in terms of parameters $\boldsymbol{\theta}$. We assume that all constituents of $\boldsymbol{\theta}$ can be divided as follows, where $t_{\mathrm{diff}}, \bar{z}$ and T, M, R_V and A_V, and s are independent:

$$P(\boldsymbol{\theta}, T) = P(t_{\mathrm{diff}}|\bar{z}, T) P(M|\bar{z}, T) P(s|\bar{z}, T) \times P(R_V, A_V|\bar{z}, T) P(\bar{z}, T). \quad (4)$$

The assumed independence of the parameters is certainly an oversimplification. For example, one would expect the stretch and magnitude parameters to be correlated (although the true values of these two parameters should be independent of t_{diff}, R_V, and A_V). Ignoring the correlation might conceivably lead to an overestimation of the probabilities for very bright SNe Ia with a small stretch parameter, or very dim SNe Ia with a large stretch parameter. However, we are exploring every possible combination of stretch and magnitude parameters; the "correct" combination should naturally be a better "fit" to the data, thus acquiring a larger weight than all the other ones.

The prior $P(\bar{z}, T)$ includes the relative rates of the various SN types as a function of redshift. Unfortunately, these rates are not well known, especially at high redshift. We thus consider three different models for the ratio of the CC SN rates to the SN Ia rates. The models are based on Dahlen & Fransson (1999) and shown in Figure 3. They correspond to three different values of the characteristic time delay parameter τ: $\tau = 1, 2$, and 3 Gyr. Based on Dahlen & Fransson (1999), we also assume that the relative (rounded off) fractions of the CC SNe are $f_{\mathrm{Ibc}} = 0.27$, $f_{\mathrm{IIL}} = 0.35, f_{\mathrm{IIp}} = 0.35$, and $f_{\mathrm{IIn}} = 0.02$, for all three models, regardless of the redshift.

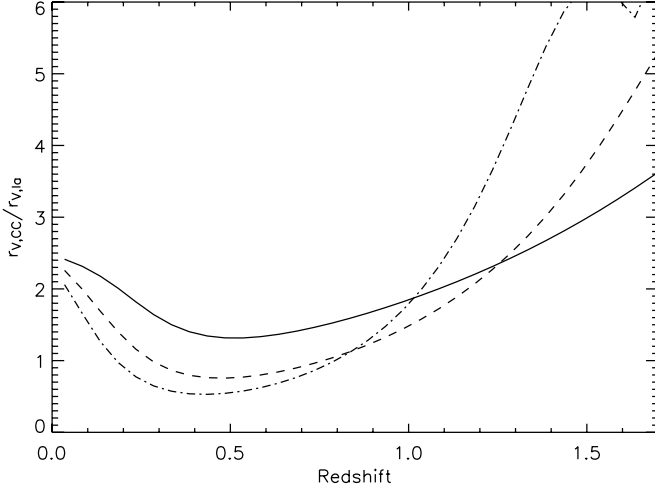[20] See http://supernova.lbl.gov/~nugent/nugent_templates.html.

Fig. 3.—Three models for the ratio of the CC/Type Ia rates as a function of redshift based on Dahlen & Fransson (1999). The solid line is for the time delay parameter $\tau = 1$ Gyr, the dashed line is for $\tau = 2$ Gyr, and the dot-dashed line is for $\tau = 3$ Gyr.

Note that the usage of these models does not bias our answer in any way, as we are not making any assumptions about the *absolute* rates of SNe, but only about their relative rates. If we assume all three models to be equally likely, then the probability density $P(T)$ of observing an SN of type T for assumption n about the relative rates of the CC SNe to SNe Ia is given by

$$P(\bar{z}, T) = \frac{R_n(\bar{z}, T)}{\sum_{l=1}^{N_{\text{models}}} R_l(\bar{z}, T)}, \qquad (5)$$

where $R_n(\bar{z}, T)$ is the rate of type T SNe for model n and $N_{\text{models}} = 3$.

The difference in the dates of maximum light between the template and the data, t_{diff}, can also take on any value, making the prior $P(t_{\text{diff}}|T)$ flat. In practice, we shift the relative dates of maximum between the measured and the template light curves by increments of 1 day. The marginalization of this parameter thus amounts to a sum over a finite number (which we take to be 160) of such shifts:

$$P(t_{\text{diff}}|\bar{z}, T) = \frac{1}{t_{\text{diff}}^{\max} - t_{\text{diff}}^{\min}}, \qquad (6)$$

where the maximum $t_{\text{diff}}^{\max}$ and minimum $t_{\text{diff}}^{\min}$ set the limits on t_{diff}.

The priors on $P(M|\bar{z}, T)$ and $P(s|\bar{z}, \text{Ia})$ are taken to be Gaussian:

$$P(M|\bar{z}, T) = \frac{e^{-\left(M - \bar{M}\right)^2/2\delta M^2}}{\sqrt{2\pi}\delta M}, \qquad (7)$$

$$P(s|\bar{z}, \text{Ia}) = \frac{e^{-(s - \bar{s})^2/2\delta s^2}}{\sqrt{2\pi}\delta s}. \qquad (8)$$

A table of the mean magnitudes $\bar{M}$ and the standard deviations δM, as well as the values for the mean stretch $\bar{s}$ and the standard deviation δs, is given in Kuznetsova & Connolly (2007). For reference, we extract the mean magnitudes $\bar{M}$ in the rest-frame B band from P. E. Nugent (see footnote 20) and the standard deviations, δM, from Richardson et al. (2002). The stretch parameters are extracted from Sullivan et al. (2006b). Note that for non–Type Ia SNe, a complete set of "virtual" values for the stretch parameters are inserted into equation (8) and then marginalized with a flat prior (see Appendix B in Kuznetsova & Connolly 2007).

The effects of interstellar extinction are difficult to parameterize due to a lack of generally accepted models for the behavior of the Cardelli-Clayton-Mathis parameters A_V and R_V. We compromise by considering a case of no extinction and two cases of extinction with a moderate value of $A_V = 0.4$ and two different values of R_V, 2.1 and 3.1. The mathematical framework used in the analysis easily allows for the implementation of real distributions for A_V and R_V, once they become standardized. It is known that in simulations A_V is sharply peaked near 0 (e.g., Hatano et al. 1998; for more recent treatment, see also Riello & Patat 2005); therefore, not considering very large values of A_V is reasonable. All three cases ($N_V = 3$) are considered equally possible. In other words, we take

$$P(R_V, A_V|\bar{z}, T) = \frac{1}{N_V}. \qquad (9)$$

It is certainly a simplified extinction model; however, it appears to be sufficient as demonstrated by the largely successful typing of known Type Ia candidates in two such diverse samples as the 73 SNLS-identified (Astier et al. 2006) SNe Ia and the gold and silver SNe Ia in the *HST* GOODS data (Kuznetsova & Connolly 2007). The method correctly identified 69 out of the 73 SNLS SNe Ia. For the remaining four candidates, at least one filter band included wavelengths outside of the well-understood optical range in the SN rest frame. It also correctly identified seven out of eight gold and silver SNe Ia and five out of five gold and silver CC SNe. Another consideration to note here is that extinction primarily affects the measured magnitudes, and our model already takes into account wide variations in the magnitudes (eq. [7]).

Putting everything together, we see that the numerator of equation (2) is given by

$$\int_{\boldsymbol{\theta}} P(\{D_i\}, z|\boldsymbol{\theta}, \text{Ia})P(\boldsymbol{\theta}, \text{Ia})\,d\boldsymbol{\theta}$$

$$= \sum_{\bar{z}=z_{\min}}^{z_{\max}} \frac{\Delta\bar{z}}{\sqrt{2\pi}\delta z} e^{-(z-\bar{z})^2/2\delta z^2} \frac{1}{\sum_{l=1}^{N_{\text{models}}} R_l(\bar{z}, T)}$$

$$\times \sum_{n=1}^{N_{\text{models}}} R_n(\bar{z}, \text{Ia}) \frac{1}{N_V} \sum_{n_v=1}^{N_V} \Delta N_v$$

$$\times \sum_{M=M_{\min}}^{M_{\max}} \frac{\Delta M}{\sqrt{2\pi}\delta M} e^{-\left(M-\bar{M}\right)^2/2\delta M^2} \frac{\Delta t_{\text{diff}}}{t_{\text{diff}}^{\max} - t_{\text{diff}}^{\min}}$$

$$\times \sum_{s=s_{\min}}^{s_{\max}} \frac{\Delta s}{\sqrt{2\pi}\delta s} e^{-(s-\bar{s})^2/2\delta s^2} \prod_{i=1}^{n_{\text{epochs}}} \frac{\exp\left[-\left(\bar{D}_j - D_i\right)^2/2\delta D_i^2\right]}{\sqrt{2\pi}\delta D_i} \qquad (10)$$

for SNe Ia, and for types T' that are non–Type Ia SNe, it is

$$\int_{\boldsymbol{\theta}} P(\{D_i\}, z|\boldsymbol{\theta}, T')P(\boldsymbol{\theta}, T')\,d\boldsymbol{\theta}$$

$$= \sum_{\bar{z}=z_{\min}}^{z_{\max}} \frac{\Delta\bar{z}}{\sqrt{2\pi}\delta z} e^{-(z-\bar{z})^2/2\delta z^2} \frac{1}{\sum_{l=1}^{N_{\text{models}}} R_l(\bar{z}, T)}$$

$$\times \sum_{n=1}^{N_{\text{models}}} R_n(\bar{z}, T') \frac{1}{N_v} \sum_{n_v=1}^{N_v} \Delta N_v$$

$$\times \sum_{M=M_{\min}}^{M_{\max}} \frac{\Delta M}{\sqrt{2\pi}\delta M} e^{-\left(M-\bar{M}\right)^2/2\delta M^2} \frac{\Delta t_{\text{diff}}}{t_{\text{diff}}^{\max} - t_{\text{diff}}^{\min}}$$

$$\times \prod_{i=1}^{n_{\text{epochs}}} \frac{\exp\left[-\left(\bar{D}_j - D_i\right)^2/2\delta D_i^2\right]}{\sqrt{2\pi}\delta D_i}. \qquad (11)$$

In equations (10) and (11), we marginalize over parameters $\boldsymbol{\theta}$, approximating the integration by summation. The range of redshifts $[z_{\min}, z_{\max}]$ is taken to be from 0 to 1.7 in the denominator of equation (2) and over a bin of interest in the numerator (this point is explained in more detail later in this section), and we take $\Delta z = 0.05$. The mean values of z and the error on the z, δz, are given in Tables 4, 5, 6, and 7 for the candidates used in the analysis. The value of Δt_{diff} is 1 day, and $\Delta N_v = 1$. We sum M from $M_{\min} = -3\delta M$ to $M_{\max} = +3\delta M$ with a total of 12 steps, and we sum s from $s_{\min} = 0.65$ to $s_{\max} = 1.3$ in 14 steps. For non–Type Ia SNe, a complete set of virtual values for the stretch parameters are inserted into equation (8) and then marginalized with a flat prior (see Appendix B in Kuznetsova & Connolly 2007).

The probability that the αth candidate is an SN Ia belonging to the jth redshift bin, $[\bar{z}_{j,\mathrm{lower}}, \bar{z}_{j,\mathrm{upper}}]$, is thus

$$P_j^\alpha = \frac{\int_{\bar{z}_{j,\mathrm{lower}}}^{\bar{z}_{j,\mathrm{upper}}} d\bar{z} \int_{\boldsymbol{\theta}} P(\{D_i\}, z | \boldsymbol{\theta}, \mathrm{Ia}) P(\boldsymbol{\theta}, \mathrm{Ia}) \, d\boldsymbol{\theta}}{\sum_T \int_0^\infty d\bar{z} \int_{\boldsymbol{\theta}} P(\{D_i\}, z | \boldsymbol{\theta}, T) P(\boldsymbol{\theta}, T) \, d\boldsymbol{\theta}}. \quad (12)$$

Let us now introduce the following variables:

1. N_j is the total count of the candidates contributing to the jth redshift bin.
2. P_j^α is the Bayesian probability for each candidate α in the jth redshift bin ($\alpha = [1, \ldots, N_j]$).
3. $\{P^\alpha\}_j$ is the full set of probabilities for the candidates in the jth redshift bin.
4. d_j is the most likely number of Type Ia candidates in the jth redshift bin.

Our goal is to find d_j, as well as the error on this number, given N_j and P_j^α values.

If N_j is large, say, of order 100 (which is the case for our Monte Carlo samples), then d_j can be simply evaluated as

$$d_j = \sum_{\alpha=1}^{N_j} P_j^\alpha, \quad (13)$$

where the uncertainty on d_j is given by the square root of the binomial and Poisson variances:

$$\Delta d_j = \sqrt{\sum_{\alpha=1}^{N_j} P_j^\alpha \left(1 - P_j^\alpha\right) + \sum_{\alpha=1}^{N_j} P_j^\alpha}. \quad (14)$$

Note that if all of the probabilities P_j^α were 1 (i.e., the candidates were all known to be SNe Ia), using equation (13) would amount to a simple counting of the number of candidates, and equation (14) would become the usual $N_j^{1/2}$ error for a large number of events N_j.

For a small number of events, $N_j < 10$, which is typically the case for our data samples, using equations (13) and (14) would be incorrect. A more sophisticated approach is needed. Let us define a variable x_α such that $x_\alpha = 1$ if the αth candidate is indeed a Type Ia and $x_\alpha = 0$ if it is not, so that there are $k_j \equiv \sum_{\alpha=1}^{N_j} x_\alpha$ SNe Ia in this bin. The probability to obtain d_j is given by

$$P\left(d_j | \{P^\alpha\}_j\right) = \sum_{\{x_\alpha\}} P(d_j | \{x_\alpha\}) P\left(\{x_\alpha\} | \{P^\alpha\}_j\right) \quad (15)$$

$$= \sum_{\{x_\alpha\}} \frac{P(\{x_\alpha\} | d_j) P(d_j)}{\int_{d_j=0}^\infty P(\{x_\alpha\} | d_j) P(d_j) \, d(d_j)}$$

$$\times P\left(\{x_\alpha\} | \{P^\alpha\}_j\right), \quad (16)$$

where the sum on d_j can, in principle, extend to arbitrarily large values (for example, if $N_j = 2$, there is still a small but nonzero probability that d_j can be 100). We assume a flat prior for $P(d_j)$, in which case the denominator integrates to unity.

The first term in equation (16) is a normalized Poisson distribution for the expected d_j number of events while $k_j = \sum_{\alpha=1}^{N_j} x_\alpha$ events are assumed to be in the jth bin:

$$P(\{x_\alpha\} | d_j) = \frac{d_j^{k_j} e^{-d_j}}{k_j!}, \quad k_j = \sum_{\alpha=1}^{N_j} x_\alpha. \quad (17)$$

The term $P(\{x_\alpha\} | \{P^\alpha\}_j)$ in equation (16) is the probability that certain SNe do or do not occupy the jth bin. This probability is simply

$$P\left(\{x_\alpha\} | \{P^\alpha\}_j\right) = \prod_{\alpha=1}^{N_j} \left[P_j^\alpha x_\alpha + \left(1 - P_j^\alpha\right)(1 - x_\alpha)\right]. \quad (18)$$

Because we have no way of knowing a priori which candidate belongs in the jth bin, we must sum over all possible $\{x_\alpha\}$ values:

$$P\left(d_j | \{P^\alpha\}_j\right) = \sum_{\{x_\alpha\}} \frac{d^{k_j} e^{-d_j}}{k_j!} \prod_{\alpha=1}^{N_j} \left[P_j^\alpha x_\alpha + \left(1 - P_j^\alpha\right)(1 - x_\alpha)\right]. \quad (19)$$

To obtain the best estimate for d_j, we must maximize $P(d_j | \{P^\alpha\}_j)$ given in equation (19). In practice, this is done numerically for a range of test d_j values from 0 to some maximum $d_{j,\max}$ (we arbitrarily take it to be 50) to find out which d_j maximizes the probability.

Let us consider an example. Suppose that we have two SNe in a given bin, with probabilities of being SNe Ia given by $P^1 = 0.8$ and $P^2 = 0.9$. The possible permutations of x_α values would be $(0, 0)$, meaning that neither candidate is a Type Ia; $(0, 1)$ and $(1, 0)$, meaning that only one candidate is a Type Ia; and $(1, 1)$, meaning that both candidates are Type Ia. Then we need to maximize

$$\frac{d^0 e^{-d}}{0!}(1 - 0.8)(1 - 0.9) + \frac{d^1 e^{-d}}{1!} 0.8(1 - 0.9)$$

$$+ \frac{d^1 e^{-d}}{1!}(1 - 0.8)0.9 + \frac{d^2 e^{-d}}{2!} 0.8 \times 0.9 \quad (20)$$

as a function of d. For this particular example, the best estimate for the number of SNe Ia is in fact $1.68^{+2.62}_{-0.58}$, where the errors are estimated as described below.

To evaluate the uncertainty on d_j, we find the 68% confidence regions for d_j, $[d_j - \sigma_{j,\mathrm{low}}, d + \sigma_{j,\mathrm{high}}]$, by solving

$$16\% = \int_0^{d_j - \sigma_{j,\mathrm{low}}} P\left(d_j | \{P^\alpha\}_j\right) d(d_j)$$

$$= \int_{d+\sigma_{j,\mathrm{high}}}^\infty P\left(d_j | \{P^\alpha\}_j\right) d(d_j). \quad (21)$$

In the case where $d_j \ll 1$, we set $\sigma_{j,\mathrm{low}} = 0$ and find $\sigma_{j,\mathrm{high}}$ by satisfying

$$32\% = \int_{\sigma_{j,\mathrm{high}}}^\infty P\left(d_j | \{P^\alpha\}_j\right) d(d_j). \quad (22)$$

We assume that all candidates whose redshift is within $\pm 3\delta z$ of the jth bin's boundaries (where δz is the uncertainty on the candidates' redshift, listed in Tables 4, 5, 6, and 7) will contribute to this bin. Note that in this formulation, a single candidate with a poorly known redshift may have a probability distribution that spans several redshift bins.

We calculate $P(\mathrm{Ia}|\{D_i\}, z)$ for all 57 candidates. If a given candidate's $P(\{D_i\}, z|\boldsymbol{\theta}, T)P(\boldsymbol{\theta}, T)$ is less than 10^{-15} for all types T, it is considered to be an "anomaly" and is excluded from further consideration. The 10^{-15} cut was chosen because it is much smaller than the values calculated for simulated SNe in the Monte Carlo. This method thus excludes any need for the often subjective and time-consuming decision on whether or not a candidate might be an SN of a given type; all dubious candidates are weighted appropriately and left in the sample for the probability to decide.

It is a good sanity check to examine the values of $P(\mathrm{Ia}|\{D_i\}, z)$ for the gold and silver Type Ia candidates from Riess et al. (2004b). Tables 4, 5, 6, and 7 list $P(\mathrm{Ia}|\{D_i\}, z)$ (with $[\bar{z}_{j,\mathrm{lower}}, \bar{z}_{j,\mathrm{upper}}] = [0.0, 1.7]$) for all of the candidates. Several candidates have "N/A" listed for $P(\mathrm{Ia}|\{D_i\}, z)$: these are the "anomalous" candidates, as described above. It is apparent that the gold and silver Type Ia candidates are among the largest contributors to a given redshift bin. All but one of them, SN 2003eb, have probabilities ≥ 0.8. SN 2003eb has only two epochs (epochs 4 and 5 of the GOODS data set) with "appreciable" S/N (>10) in both F775W and F850LP bands. One silver Type Ia candidate, SN 2003lv, appears to have a rare residual cosmic-ray contamination in the F775W band, making it appear inconsistent with any of the SN types considered. Three silver CC SNe, SN 2002kl, SN 2003bb, and SN 2002fz, have the probabilities of being SNe Ia of 0.3, 0.8, and 0.9, respectively. They are in fact most consistent with being SNe IIn; however, because the fraction of SNe IIn is heavily deweighted among CC SNe ($f_{\mathrm{IIn}} = 0.02$), their resulting $P(\mathrm{Ia}|\{D_i\}, z)$ are higher than one would have expected. How much do our assumptions about the fractions of various SN types among the CC SNe influence our answer? As seen in § 3.3.1, if we assume that all CC types are equally likely and that the ratio of the CC to Type Ia rates is redshift independent, the changes to our final results are within the quoted uncertainties.

Another sanity check is to make sure that the candidates with low $P(\mathrm{Ia}|\{D_i\}, z)$ values are not all of a particular class (e.g., SNe Ibc). We have verified that indeed they are not.

It is worth noting that variable objects other than SNe, such as AGNs, are selected during the first selection stage. If some of these objects also pass the second selection stage, they are unlikely to bias the results significantly, as the specifically designed cuts in the third stage would likely reject such candidates. As an extra check, we verified that none of the candidates listed in Tables 4, 5, 6, and 7 that are close (within 3 pixels) to the core of their host galaxies have a matching X-ray–bright object in the Chandra Deep Field catalogs (Alexander et al. 2003; Rosati et al. 2002). The only questionable candidate that might have a matching object is candidate 3 in Table 5; however, its $P(\mathrm{Ia}|\{D_i\}, z)$ never exceeds $\sim 10^{-6}$ for any redshift bin considered.

In order to estimate d_j, one must select some kind of redshift binning. One must be careful about the selection of the redshift bins in an analysis whose goal is to estimate the SN rates because the use of binning averages the behavior of the rates over the width of the bin. However, the uncertainty in the candidates' redshifts forces us to use finite bins, or, in other words, it does not make sense to use infinitely narrow bins when there is significant uncertainty in the candidate redshifts. For our analysis, we choose the width of the bins to be $\Delta \bar{z} = 0.1$. Table 8 lists the

TABLE 8

BEST ESTIMATE (I.E., THE MOST PROBABLE) NUMBER OF SNe Ia, d_j^m, IN $\Delta z = 0.1$ REDSHIFT BINS ($j = [1, \ldots, 17]$), FOR THE FOUR SAMPLES LISTED IN TABLE 2 ($m = [1, \ldots, 4]$)

Redshift Bin	d_j^1	d_j^2	d_j^3	d_j^4	Total
$0.0 \leq z < 0.1$	$0.00^{+1.13}_{-0.00}$	$0.00^{+1.13}_{-0.00}$	$0.00^{+1.13}_{-0.00}$	$0.00^{+1.13}_{-0.00}$	$0.00^{+1.13}_{-0.00}$
$0.1 \leq z < 0.2$	$0.00^{+1.13}_{-0.00}$	$0.00^{+1.13}_{-0.00}$	$0.00^{+1.13}_{-0.00}$	$0.00^{+1.13}_{-0.00}$	$0.00^{+1.13}_{-0.00}$
$0.2 \leq z < 0.3$	$0.00^{+1.13}_{-0.00}$	$0.00^{+1.13}_{-0.00}$	$0.00^{+1.13}_{-0.00}$	$0.00^{+1.13}_{-0.00}$	$0.00^{+1.15}_{-0.00}$
$0.3 \leq z < 0.4$	$0.00^{+1.17}_{-0.00}$	$0.00^{+1.41}_{-0.00}$	$0.00^{+1.13}_{-0.00}$	$0.00^{+1.13}_{-0.00}$	$0.00^{+1.45}_{-0.00}$
$0.4 \leq z < 0.5$	$0.00^{+1.83}_{-0.00}$	$1.35^{+2.77}_{-0.41}$	$0.00^{+1.14}_{-0.00}$	$0.00^{+1.13}_{-0.00}$	$1.84^{+3.13}_{-0.62}$
$0.5 \leq z < 0.6$	$1.74^{+2.94}_{-0.63}$	$0.00^{+1.45}_{-0.00}$	$0.00^{+1.16}_{-0.00}$	$0.00^{+1.13}_{-0.00}$	$1.98^{+3.12}_{-0.72}$
$0.6 \leq z < 0.7$	$3.31^{+3.28}_{-1.05}$	$0.00^{+1.44}_{-0.00}$	$0.00^{+1.19}_{-0.00}$	$0.00^{+1.13}_{-0.00}$	$3.58^{+3.45}_{-1.13}$
$0.7 \leq z < 0.8$	$2.17^{+3.13}_{-0.75}$	$0.00^{+2.00}_{-0.00}$	$0.00^{+1.29}_{-0.00}$	$1.00^{+2.28}_{-0.28}$	$3.98^{+3.72}_{-1.29}$
$0.8 \leq z < 0.9$	$1.26^{+3.02}_{-0.46}$	$1.59^{+2.95}_{-0.56}$	$0.85^{+2.42}_{-0.26}$	$0.00^{+1.13}_{-0.00}$	$4.07^{+3.78}_{-1.39}$
$0.9 \leq z < 1.0$	$2.94^{+3.21}_{-0.95}$	$0.72^{+3.09}_{-0.14}$	$0.19^{+1.85}_{-0.19}$	$0.00^{+1.28}_{-0.00}$	$4.89^{+4.00}_{-1.56}$
$1.0 \leq z < 1.1$	$0.00^{+1.31}_{-0.00}$	$0.00^{+2.09}_{-0.00}$	$0.10^{+1.85}_{-0.10}$	$0.00^{+1.61}_{-0.00}$	$1.56^{+3.37}_{-0.59}$
$1.1 \leq z < 1.2$	$1.05^{+2.37}_{-0.30}$	$0.00^{+1.92}_{-0.00}$	$0.00^{+1.15}_{-0.00}$	$0.00^{+1.46}_{-0.00}$	$1.74^{+3.09}_{-0.57}$
$1.2 \leq z < 1.3$	$1.03^{+2.34}_{-0.29}$	$0.00^{+1.69}_{-0.00}$	$0.00^{+1.13}_{-0.00}$	$0.00^{+1.17}_{-0.00}$	$1.36^{+2.78}_{-0.41}$
$1.3 \leq z < 1.4$	$1.00^{+2.28}_{-0.28}$	$0.00^{+1.66}_{-0.00}$	$1.00^{+2.28}_{-0.28}$	$0.91^{+2.29}_{-0.27}$	$3.27^{+3.55}_{-1.00}$
$1.4 \leq z < 1.5$	$0.00^{+1.13}_{-0.00}$	$0.00^{+1.59}_{-0.00}$	$0.00^{+1.13}_{-0.00}$	$0.00^{+1.13}_{-0.00}$	$0.00^{+1.59}_{-0.00}$
$1.5 \leq z < 1.6$	$0.00^{+1.13}_{-0.00}$	$0.00^{+1.44}_{-0.00}$	$0.00^{+1.13}_{-0.00}$	$0.00^{+1.13}_{-0.00}$	$0.00^{+1.44}_{-0.00}$
$1.6 \leq z < 1.7$	$0.00^{+1.13}_{-0.00}$	$0.00^{+1.27}_{-0.00}$	$0.00^{+1.13}_{-0.00}$	$0.00^{+1.13}_{-0.00}$	$0.00^{+1.27}_{-0.00}$

NOTES.—The total numbers are the results of applying the counting procedure described in the text to the combined candidates from all four samples (in other words, the total probability distribution is not a trivial sum of the probability distributions for the four samples). All the uncertainties reflect a 68% confidence region.

numbers of observed candidates in these bins, as well as their uncertainties, for the four samples listed in Table 2 (d_j^m refers to a number of candidates in the jth redshift bin for the mth sample). All the uncertainties reflect a 68% confidence region. In order to calculate the total numbers of SNe, d_j, we use the procedure described above on the combined candidates from all four samples. In other words, the total d_j is not a trivial sum of the probability distributions of the d_j^m values.

3.3.1. *Sensitivity to Varying Priors*

As usual in Bayesian analysis, the errors on the observed number of SNe d_j calculated as described in § 3.3 are a combination of statistical and systematic uncertainties. However, to gain an appreciation for the effect of the prior assumptions on the final result, we compute the change in d_j values by varying the calculation of $P(\mathrm{Ia}|\{D_i\}, z)$ from equation (2) in three different ways:

1. *Large extinction.*—In § 3.3 we considered three discrete cases for extinction: no extinction, $(A_V, R_V) = (0.4, 2.1)$, and $(A_V, R_V) = (0.4, 3.1)$. We now add the case of $(A_V, R_V) = (1.0, 3.1)$ to the extinction prior and consider it to be equally likely as the cases of no extinction and moderate extinction. It is in fact known that a value of $A_V = 1.0$ is much less likely than, say, $A_V = 0$; however, it is in cases of strong extinction that the overlap between the magnitude phase space of SNe Ia and CC SNe becomes the largest.

2. *Overluminous SNe Ibc.*—In Richardson et al. (2006) it is pointed out that there may exist a subclass of Type Ibc SNe whose mean rest-frame B-band magnitudes are much closer to those of normal SNe Ia, with $\bar{M} = -20.08$, $\delta M = 0.46$. We add these SNe as one more type to our list of SN types considered, assuming that $f_{\mathrm{Ibc}} = 0.18$ for normal SNe Ibc and 0.09 for the overluminous ones.

3. *Flat ratio of the CC to Type Ia rates, all CC types equally likely.*—Instead of using the redshift-dependent models for the ratio of the CC to Type Ia SN rates, we now assume that the ratio is redshift independent, and taken to be 2.15, which is roughly

TABLE 9
Change in the Estimates for the Numbers of SNe Ia, d_j, as a Result
of Using Alternative Priors for the $\boldsymbol{\theta}$ Parameters

Redshift Bin	$A_V = 1$	Overluminous SNe Ibc	Flat CC/Ia Rates $f_{CC} = 0.25$
$0.0 \leq z < 0.1$	0.00	0.00	0.00
$0.1 \leq z < 0.2$	0.00	0.00	0.00
$0.2 \leq z < 0.3$	0.00	0.00	0.00
$0.3 \leq z < 0.4$	0.00	0.00	0.00
$0.4 \leq z < 0.5$	0.00	-0.14	-0.32
$0.5 \leq z < 0.6$	0.29	0.93	-0.24
$0.6 \leq z < 0.7$	-0.09	-0.86	-0.21
$0.7 \leq z < 0.8$	-0.16	-0.05	-0.08
$0.8 \leq z < 0.9$	-0.04	-0.06	-0.61
$0.9 \leq z < 1.0$	0.06	-0.12	-0.56
$1.0 \leq z < 1.1$	0.14	-0.14	-0.03
$1.1 \leq z < 1.2$	0.12	0.09	0.01
$1.2 \leq z < 1.3$	-0.01	-0.02	0.00
$1.3 \leq z < 1.4$	0.09	-0.08	0.04
$1.4 \leq z < 1.5$	0.00	0.00	0.00
$1.5 \leq z < 1.6$	0.00	0.00	0.00
$1.6 \leq z < 1.7$	0.00	0.00	0.00

Note.—Listed are the differences between the d_j obtained for the alternative parameters and for the default priors, in $\Delta z = 0.1$ redshift bins ($j = [1, \ldots, 17]$), for the combination of the four samples listed in Table 2.

the average of the models shown in Figure 7 below. We also assume that the relative fractions of the CC SNe are all 0.25 ($f_{CC} = 0.25$), or, in other words, that all classes of the CC SNe are equally likely.

The considered alternative priors are deliberately taken to be such that the effect on $P(\mathrm{Ia}|\{D_i\}, z)$ should be the most dramatic, without too much regard for whether or not such priors are realistic. Table 9 lists the changes in d_j relative to the values specified in Table 8 as a result of using the alternative priors listed above.

It is clear from Table 9 that none of the alternative priors considered lead to a change in the mean that goes beyond the estimated errors in Table 8.

4. THE RATES CALCULATION

Next, we compute the expected number of candidates in the jth redshift bin whose center is $\bar{z}_j$, given a volumetric SN Ia rate in the SN rest frame, $r_{V,\mathrm{Ia}}(\bar{z})$, as a function of redshift $\bar{z}$. The expected number of candidates is different from the *measured d_j* values: it is *calculated* entirely based on Monte Carlo simulations of SNe and a given rates model:

$$d_j^{\mathrm{exp}} = \Delta \bar{z}_j \frac{r_{V,\mathrm{Ia}}(\bar{z}_j)}{1 + \bar{z}_j} \frac{\Theta}{4\pi} \frac{dV}{d\bar{z}}(\bar{z}_j)$$
$$\times \left[T_{\mathrm{Ia}}(\bar{z}_j) \epsilon_{\mathrm{Ia}}(\bar{z}_j) + \frac{r_{V,\mathrm{CC}}(\bar{z}_j)}{r_{V,\mathrm{Ia}}(\bar{z}_j)} T_{\mathrm{CC}}(\bar{z}_j) \epsilon_{\mathrm{CC}}(\bar{z}_j) \right], \quad (23)$$

where $\Delta \bar{z}_j$ is the width of the redshift bin; Θ is the survey area covered; $dV/d\bar{z}$ is the comoving volume computed assuming a ΛCDM cosmology with $\Omega_\Lambda = 0.7$, $\Omega_M = 0.3$, and $H_0 = 100\, h_{70}\, (\mathrm{km\ s^{-1}})\, \mathrm{Mpc}^{-1}$; $T_{\mathrm{Ia}}(\bar{z})$ and $T_{\mathrm{CC}}(\bar{z})$ are the control times for Type Ia and non–Type Ia candidates, respectively; ϵ_{Ia} and ϵ_{CC} are the efficiencies of the stage 3 selection for Type Ia and non–Type Ia candidates, respectively; and $r_{V,\mathrm{CC}}(\bar{z})/r_{V,\mathrm{Ia}}(\bar{z})$ is the ratio of the non–Type Ia SN rate to the Type Ia SN rate. Once again, the appearance of this ratio does not bias our results, since we do not make any assumptions about the *absolute* Type Ia rate.

The control time in equation (23) enters with a factor of $(1 + \bar{z})$. This is a consequence of the fact that it is calculated in the observer frame, as described later.

The control time T is defined as the time during which an SN search is *potentially* capable of finding SN candidates. In order to calculate it, we simulate *HST* observations of Type Ia and non–Type Ia SNe at redshifts up to 1.7, with the same sampling and exposure times as those of the real data. By shifting the observing grid along the light curves, we calculate the weighted sum of the number of days during which a given SN could be detected. The weight factors are obtained from the stage 1 efficiency parameterization; it is also required that the light curves satisfy the stage 2 S/N requirements. Therefore, stage 1 and 2 SN selection efficiencies are naturally built into the control time calculation. However, the stage 3 selection efficiency is *not* part of the control time calculation and must therefore be computed separately. Calculating the area of the survey is straightforward using a Monte Carlo approach. The calculation of the control time and the survey area is given in § 4.1.

The stage 3 selection efficiencies ϵ_{Ia} and ϵ_{CC} must be calculated for the candidates that passed the control time requirements and thus satisfy both stage 1 and 2 cuts. We create a Monte Carlo sample simulating real SN candidates of five different types and apply stage 1 and 2 cuts to them. We simulate both Type Ia and non–Type Ia candidates and calculate the number of candidates as we would for real data. This procedure is described in detail in § 4.2.

The errors on the expected d_j^{exp} are a combination of statistical and systematic uncertainties. Apart from the uncertainties inherent in the calculation of $P(\mathrm{Ia}|\{D_i\}, z)$, the dominant systematic uncertainties come from two sources: estimating the variation in the control time for SNe Ia for values of the light-curve timescale stretch, s, other than 1, and estimating the effect of varying the ratio of the rates $r_{V,\mathrm{CC}}(\bar{z})/r_{V,\mathrm{Ia}}(\bar{z})$. The former is described in more detail in § 4.1, and for the latter we use two models described in § 3.3, for $\tau = 1$ and 3 Gyr.

4.1. *The Control Time and Search Area Calculation*

Let us start with describing the calculation of the control time and search area, T and Θ from equation (23). The control time is the time during which an SN search is in principle capable of finding SN candidates on the area covered. For the GOODS fields, the orientation of the tiles is such that a candidate is not necessarily accessible for every search epoch due to edge effects (see Fig. 1). For example, for sample 1 from Table 2, a given location may only be covered by epochs 1, 3, and 5 (but not by epochs 2 and 4) of the GOODS-N data set. In both our control time calculation and the search area calculation, we thus consider all of the possible epoch permutations at each location: 31 possible permutations for samples 1, 3, and 4 and 15 possible permutations for sample 2.

We perform separate control time and search area calculations for the four samples listed in Table 2; however, the approach is the same. For the control time calculation, we make use of the simulation described in some detail in Appendix A of Kuznetsova & Connolly (2007). We use it to create simulated *HST* observations in both F775W and F850LP bands for SNe Ia of stretch 1, as well as for non–Type Ia SNe, at redshifts up to 1.7 with an increment of 0.1. Separate sets of observations are generated for each possible permutation of the available search epochs, for each of the four samples. For example, for an SN from sample 1 that happens to be present in every one of the GOODS-N epochs, there will be five simulated search observations and a single reference observation. We use typical epoch

TABLE 10

Type Ia Control Time as a Function of Redshift, for the Configurations on which a Supernova Candidate
is Assumed to be Present on All of the Search Epochs

	Control Time (yr)											
	Sample 1			Sample 2			Sample 3			Sample 4		
$\bar{z}$	$s=1$	$s=0.65$	$s=1.3$	$s=1$	$s=0.65$	$s=1.3$	$s=1$	$s=0.65$	$s=1.3$	$s=1$	$s=0.65$	$s=1.3$
0.1............	0.84	0.78	0.84	0.84	0.66	0.85	0.68	0.65	0.68	0.30	0.27	0.35
0.2............	0.84	0.77	0.84	0.84	0.65	0.85	0.68	0.63	0.67	0.32	0.29	0.42
0.3............	0.85	0.77	0.85	0.83	0.64	0.85	0.68	0.63	0.67	0.31	0.28	0.37
0.4............	0.84	0.75	0.83	0.80	0.61	0.84	0.67	0.60	0.66	0.32	0.28	0.36
0.5............	0.84	0.73	0.84	0.77	0.59	0.84	0.67	0.58	0.66	0.32	0.28	0.36
0.6............	0.83	0.72	0.84	0.73	0.56	0.82	0.66	0.57	0.65	0.33	0.28	0.37
0.7............	0.81	0.68	0.84	0.69	0.53	0.79	0.63	0.53	0.64	0.32	0.29	0.37
0.8............	0.78	0.64	0.83	0.64	0.51	0.75	0.59	0.49	0.63	0.33	0.29	0.37
0.9............	0.72	0.59	0.80	0.57	0.46	0.66	0.53	0.43	0.58	0.33	0.28	0.37
1.0............	0.68	0.57	0.75	0.54	0.43	0.62	0.48	0.36	0.54	0.33	0.28	0.36
1.1............	0.65	0.55	0.72	0.51	0.40	0.59	0.46	0.32	0.49	0.32	0.27	0.37
1.2............	0.63	0.53	0.69	0.48	0.35	0.56	0.42	0.27	0.47	0.32	0.26	0.36
1.3............	0.60	0.49	0.67	0.46	0.30	0.55	0.38	0.22	0.45	0.32	0.25	0.36
1.4............	0.57	0.42	0.64	0.44	0.23	0.53	0.37	0.17	0.43	0.31	0.20	0.36
1.5............	0.56	0.36	0.62	0.39	0.15	0.48	0.32	0.13	0.40	0.31	0.17	0.35
1.6............	0.51	0.24	0.59	0.34	0.09	0.44	0.27	0.09	0.37	0.26	0.11	0.34
1.7............	0.47	0.17	0.56	0.21	0.04	0.38	0.25	0.06	0.33	0.25	0.07	0.31

Notes.—The control time is given for three different values of the stretch parameter s: 1 (nominal), 0.65, and 1.30. Note that this control time has the stage 1 and 2 efficiencies built into the calculation.

separations and exposure times for a given sample. The observations are realized using an aperture exposure time calculator with a 0.1″ radius. We initially set the explosion date of the SN on the last date of the available search epoch observation set (e.g., for the SN example mentioned above it would be on the date the last of the GOODS-N data were taken). The observing grid for the search observations is then shifted by 1 day, and the procedure is repeated $N_{\rm shifts} = 350$ times (that is, spanning approximately 1 yr, which is the longest separation between the search and reference data for our data samples). For each such shift, we require that the simulated data satisfy both the stage 1 and stage 2 requirements listed in Table 3. The resulting control time thus has stage 1 and 2 efficiencies automatically included. It is given by

$$T = \sum_{k=1}^{N_{\rm shifts}} \left\{ 1 - \prod_{i=1}^{N_{\rm ep}} \left[1 - \epsilon_i^k (\mathrm{S/N}_i) \right] \right\} e_k, \qquad (24)$$

where the sum is over all the shifts; $N_{\rm ep}$ is the number of available search epochs (in the example considered above, $N_{\rm ep} = 5$); ϵ_i^k is a function of the ith subtraction's S/N, parameterized as in equation (1); and e_k is a binary quantity,

$$e_k = 1 \ (0) \qquad (25)$$

if the kth shift configuration satisfies (does not satisfy) stage 2 requirements, that assesses whether a given configuration has enough epochs with sufficient S/N for the stage 2 selection.

We repeat the control time calculation for SNe Ia with the light-curve timescale stretch values of $s = 0.65$ and 1.30, weight the results by the probability of obtaining such stretches taken from equation (8), and take the larger error between the control time computed for these stretch parameters and that computed for a stretch of 1 as a measure of the systematic error on the control time for SNe Ia. For reference, Table 10 lists the control time

as a function of redshift for both the nominal stretch of 1 and the stretch of 0.65 and 1.30, for the configurations in which an SN candidate is assumed present on all of the search epochs.

Calculating the search area is nontrivial because of the complicated orientations of the GOODS tiles, as well as the overlaps between the tiles (see Fig. 1). In addition, the search area must be calculated separately for all of the possible epoch configurations, as described above. We perform this calculation using a Monte Carlo method. First, we create a 300×300 point grid between the minimum and maximum right ascensions (α) and declinations (δ) covering the entire GOODS-N or GOODS-S area (e.g., from $\alpha = 12^{\rm h}35^{\rm m}34.85^{\rm s}$ and $\delta = 62°04'59.45''$ to $\alpha = 12^{\rm h}38^{\rm m}14.7^{\rm s}$ and $\delta = 62°23'36.78''$ for epochs 1, 3, and 5 of sample 1). Then, for a given epoch, and for each point i on the grid, we check whether this (α_i, δ_i) belongs to any of the images that were used to make subtracted data for this epoch. In other words, we convert (α_i, δ_i) into image coordinates (x_j, y_j) and check that (1) the point falls within the confines of at least one search/reference image pair, (2) it does not fall into the gap between the two ACS chips on the search image, and (3) it does not fall on a known bad pixel or a pixel that has been masked off for any other reason (e.g., due to a residual cosmic-ray contamination) on either image, although because of the drizzling there are very few affected pixels. If all of these requirements are satisfied, the point is counted toward the area calculation. Once counted, a given point can never again be counted for this particular epoch. This avoids double counting, an issue particularly important since most GOODS tiles overlap at least somewhat with their immediate neighbors, and a point with a given (α_i, δ_i) may well be present on several images. A separate accounting of the number of points is kept for each epoch permutation. For example, let us suppose that the number of points that cover all five of the GOODS-N epochs is a_1 and that the number of total points tried in the grid is A_1; then the area corresponding to this configuration is $S a_1 / A_1$, where S is the area of the entire GOODS-N survey.
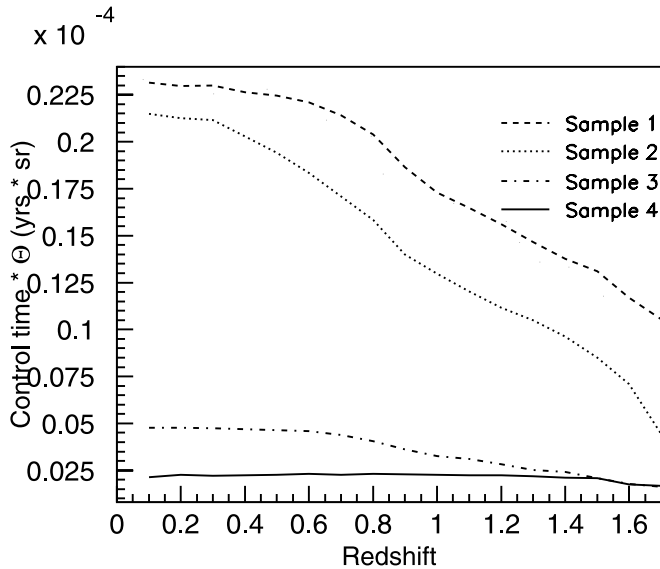
Fig. 4.—Product of the control time and surveyed area as a function of redshift for the four samples listed in Table 2, calculated for a stretch 1 SN Ia. The dashed line is for sample 1, where the five GOODS-N epochs were used as the search data, and the combined 2004 ACS sample, as the reference. The dotted line is for sample 2, where the four epochs of the 2004 ACS data set were used as the search data, and the combined GOODS-N data, as the reference. The dot-dashed line is for sample 3, where all five epochs of the GOODS-S sample were used as the search data, and the combined epochs 4+5 of the GOODS-S data set, as the reference. The solid line is for sample 4, where all five epochs of the GOODS-S sample were used as the search data, and the combined epochs 1+2 of the GOODS-S data set, as the reference.

Figure 4 shows the resulting product of the control time and surveyed area $[\Theta T(\bar{z}) = \sum_{i=1}^{n} \Theta_i T_i(\bar{z})$, where n is the number of all possible permutations] for stretch 1 SNe Ia, as a function of redshift for the four different samples in Table 2.

There are several interesting features in Figure 4. First, the product of the control time and area tends to decrease with redshift. This is a consequence of the fact that it becomes more difficult to satisfy the stage 2 S/N requirements for higher redshift (dimmer) SNe. Second, for a given redshift, the product is smaller for sample 2 than for sample 1, a consequence of the fact that there are only four search epochs in sample 2 versus five search epochs in sample 1. Third, the product is distinctly smaller for

the GOODS-S samples (samples 3 and 4) than for either of the GOODS-N samples (samples 1 and 2), a reflection of the fact that for these samples we are forced to use references made from two of the GOODS-S data set's own epochs. Finally, the product is smaller for sample 4, which uses epochs 1+2 of the GOODS-S data set as its reference data, than it is for sample 5, which uses epochs 4+5. This is simply because the rise time of an SN is smaller than its decline time.

4.2. Calculating ϵ_{Ia} and ϵ_{CC}

In order to determine the efficiency of the stage 3 selection, we generate four Monte Carlo data sets simulating the data from the four data sets listed in Table 2 (in other words, they have the same sampling, exposure times, etc., as the data). Each Monte Carlo data set contains 500 candidates for each of the five SN types considered (Ia, Ibc, IIL, IIP, and IIn). The redshifts of these candidates are drawn from a Gaussian distribution that uses the redshifts and redshift errors of the real data events; the exposure times and sampling intervals also mimic those of the real data. The candidates' rest-frame B-band magnitudes, stretch (for SNe Ia), and extinction parameters are drawn from the appropriate distributions used in equations (10) and (11). The time period between the date of explosion and the first observation is randomly drawn from a flat distribution. In addition, because we are simulating a data set as it would appear by the time it is ready for the stage 3 selection, we impose the same selection requirements from stages 1 and 2 on these Monte Carlo events as we do on the real data.

After these Monte Carlo samples are generated, we calculate the number of candidates in each redshift bin. Dividing this number by the total number of the generated SNe Ia yields the efficiency $\epsilon_{j,Ia}^{m}$, for redshift bin j for Monte Carlo data set m. Similarly, the efficiency for non–Type Ia candidates, $\epsilon_{j,CC}^{m}$, is defined as the sum of the probabilities of the non–Type Ia candidates divided by the total number of all generated non–Type Ia SNe. The values of $\epsilon_{j,Ia}^{m}$ range from ~10% to 90%, and the values of $\epsilon_{j,CC}^{m}$ range from ~3% to 50%, depending on the redshift bin.

4.3. Comparison of Expected and Observed Numbers of Supernovae

We can now put everything together and compute the expected numbers of SNe for a given model of the SN Ia rates using equation (23). We calculate the observed numbers of SNe for redshifts $\bar{z} \leq 1.7$, as well as the expected numbers of SNe
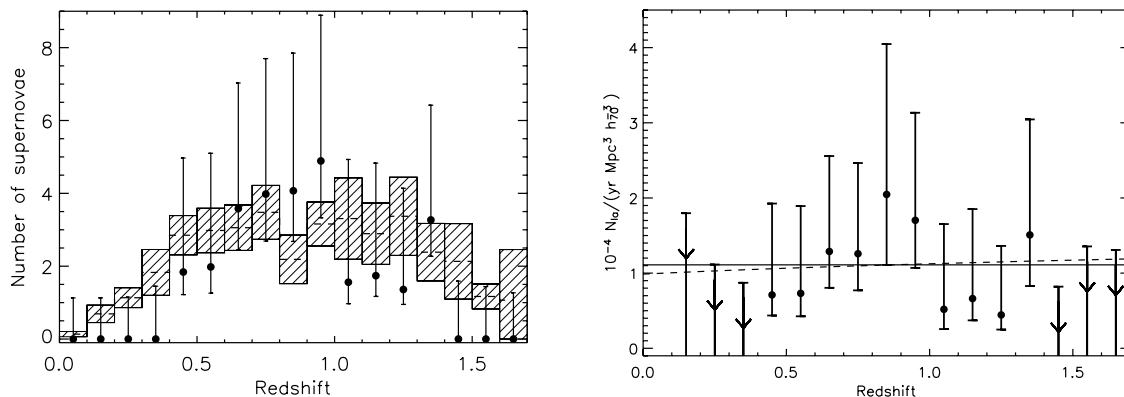

Fig. 5.—*Left*: Total observed candidates for the four samples as a function of redshift (*filled circles*). The errors on the observed candidates are given in Table 8. The predicted number of candidates has been computed assuming a redshift-independent volumetric Type Ia rate of $r_{V,Ia}(\bar{z}) = 1.1 \times 10^{-4} N_{Ia}/(\mathrm{yr}\ \mathrm{Mpc}^3\ h_{70}^{-3})$ and is plotted as a dashed histogram. The shaded region around the predicted numbers indicates the range of combined statistical and systematic errors. The contributions from the statistical and systematic errors are comparable. *Right*: Calculated rates as a function of redshift (*filled circles*), with overplotted fit results to the fits described in the text: redshift-independent rate (*solid line*) and power-law redshift-dependent rate (*dashed line*). Note that the plot does not show the rates in the first redshift bin; this is because in this bin the rates are effectively unconstrained on the scale shown.

TABLE 11

Best Estimate (i.e., the Most Probable) Number of SNe Ia, d_j^m, in $\Delta \bar{z} = 0.4$ (0.3 for the Last Bin) Redshift Bins ($j = [1, \ldots, 4]$), for the Four Samples Listed in Table 2 ($m = [1, \ldots, 4]$)

Redshift Bin	d_j^1	d_j^2	d_j^3	d_j^4	Total
$0.2 \leq z < 0.6$	$2.40^{+3.07}_{-0.86}$ (0)	$1.81^{+3.05}_{-0.60}$ (0)	$0.00^{+1.17}_{-0.00}$ (0)	$1.00^{+2.28}_{-0.28}$ (2)	$5.44^{+3.90}_{-1.63}$
$0.6 \leq z < 1.0$	$13.40^{+8.28}_{-5.22}$ (6)	$3.85^{+3.47}_{-1.25}$	$1.71^{+2.90}_{-0.63}$ (2)	$1.07^{+2.42}_{-0.30}$ (2)	$18.33^{+4.62}_{-4.62}$
$1.0 \leq z < 1.4$	$3.23^{+3.07}_{-0.97}$ (3)	$2.01^{+3.25}_{-0.75}$	$1.50^{+2.74}_{-0.48}$ (1)	$1.70^{+2.62}_{-0.58}$ (1)	$8.87^{+3.13}_{-2.36}$
$1.4 \leq z < 1.7$	$0.00^{+1.13}_{-0.00}$ (0)	$0.35^{+1.72}_{-0.35}$	$0.00^{+1.13}_{-0.00}$ (1)	$0.00^{+1.13}_{-0.00}$ (1)	$0.35^{+1.72}_{-0.35}$

Notes.—The numbers in parentheses are the number of gold and silver SNe Ia in the sample from Riess et al. (2004b) that were used in the rates analysis of Dahlen et al. (2004). The total numbers are the results of applying the counting procedure described in the text to the combined candidates from all four samples (in other words, the total probability distribution is not a trivial sum of the probability distributions for the four samples). All the uncertainties reflect a 68% confidence region.

for the two models considered in Pain et al. (2002): a redshift-independent one and one evolving with redshift as a power law. We perform a least-squares fit of the observed numbers of SNe to the predictions for both models. We also perform a maximum likelihood fit and compare the results:

1. *Redshift-independent rate.*—Assuming that the rate is flat as a function of redshift, we obtain the best-fit value of $r_{V,\mathrm{Ia}} = (1.1^{+0.2}_{-0.2}) \times 10^{-4} N_{\mathrm{Ia}}/(\mathrm{yr}\ \mathrm{Mpc}^3\ h_{70}^{-3})$, with a $\chi^2 = 11.5$ for 16 degrees of freedom. The left panel of Figure 5 shows the resulting distribution of the predicted and observed numbers of SNe. The errors on the predicted numbers of SNe are a quadratic combination of the statistical and systematic errors (the statistical and systematic errors are comparable). The maximum likelihood method yields $r_{V,\mathrm{Ia}} = (0.7^{+0.2}_{-0.2}) \times 10^{-4} N_{\mathrm{Ia}}/(\mathrm{yr}\ \mathrm{Mpc}^3\ h_{70}^{-3})$, consistent with the χ^2 method.

2. *Rate evolving as a power law with redshift.*—Assuming that the rate is varying as a function of redshift as $(1 + \bar{z})^{\alpha}$, using the χ^2 fitter we obtain the best-fitting value for $\alpha = 0.2^{+0.7}_{-0.7}$ with a $\chi^2 = 11.4$ for 15 degrees of freedom. This is consistent with Pain et al. (2002), who found $\alpha = 0.8 \pm 1.6$. Note that the fit results are also consistent with the $\alpha = 0$ case that was considered above. The maximum likelihood method yields $\alpha = -0.4^{+1.0}_{-1.1}$.

Both the redshift-independent model and the power-law model yield acceptable fit results, judging by the obtained χ^2 values (note, however, that the data points in neighboring bins are correlated, leading to lower χ^2 per dof). The probability $p(\Delta \chi^2 | \Delta \mathrm{dof}) = 0.1$, where $\Delta \chi^2$ and $\Delta \mathrm{dof}$ are the difference in the χ^2 and the numbers of degrees of freedom, respectively, for the redshift-independent model and the power-law model. In other words, the approximate probability that data would fluctuate from the redshift-independent model to the power-law model is 0.1. This fact indicates that our description of the experiment is good at both low and high redshifts. One must note, however, that at redshifts >1 the samples start becoming sparser, and at redshifts >1.4 the measurement becomes particularly difficult with this data set.

5. COMPARISON TO RATES IN THE LITERATURE

To compare our results with those of Dahlen et al. (2004), we now compute the SN Ia rates in four large redshift bins, $0.2 \leq \bar{z} < 0.6$, $0.6 \leq \bar{z} < 1.0$, $1.0 \leq \bar{z} < 1.4$, and $1.4 \leq \bar{z} < 1.7$. Table 11 enumerates the estimates for the number of candidates in these redshift bins for the four samples listed in Table 2.

Using all four samples, we can now compute the rates for each bin using equation (23). The values for $\Theta T(\bar{z})$, $dV/d\bar{z}$, $r_{V,\mathrm{CC}}/r_{V,\mathrm{Ia}}$, and $\bar{z}$ are taken in the middle of the bin. The errors on the rates are a quadratic combination of the errors on the number of observed SNe Ia listed in Table 11, as well as statistical and systematic

errors on the right-hand side of equation (23). The resulting rates are summarized in Table 12 and plotted in Figure 6 together with the rates from Dahlen et al. (2004) and results from the literature at lower redshifts. It is apparent that our results are consistent with those from the literature: in particular, at higher redshifts our rates are not inconsistent with those of Dahlen et al. (2004) although obtaining a precise measure of the consistency would require a careful evaluation of the correlations between the samples used in both analyses.

Note that SNe Ia that we have considered encompass a wide range of magnitudes, stretch parameters, extinction possibilities, etc. Therefore, the procedure described in § 3.3 accounts for not only the more standard SNe Ia (such as those described in Branch et al. 1993) but also nonstandard SNe Ia, such as SN 1991bg and SN 1991T (Filippenko et al. 1992). SN 1991bg–like SNe have low values of the stretch parameter ($s = 0.71 \pm 0.05$) and are typically ~1.7 mag fainter in the V band and ~2.6 mag fainter in the B band. Stretch values of 0.71 are certainly within the range of the stretch parameters we considered; as for the magnitudes, it is reassuring to note that the case of strong extinction ($A_V = 1$) did not significantly alter our results (see Table 9). SN 1991T–like SNe are about 0.5–0.9 mag brighter than normal SNe Ia, with stretch $s = 1.07 \pm 0.06$. Both the stretch and the magnitude values are well within the considered ranges of these parameters. Note also that the fact that the Bayesian classification method was able to accurately type the vast majority of the 73 Type Ia candidates from the SNLS data set, as was demonstrated in Kuznetsova & Connolly (2007), shows that the method is capable of identifying SNe Ia in large populations that presumably include nonstandard SNe Ia.

It is particularly interesting to compare our rate results with those of Dahlen et al. (2004). That study also analyzed the GOODS sample, but there are important differences in our methods, as pointed out above (§ 1). While our results are in statistical agreement, our measured rate in a given bin can differ from theirs

TABLE 12

SN Ia Rates in the Four Redshift Bins Considered

Redshift Bin	$r_{V,\mathrm{Ia}}(\bar{z})$ $[10^{-4} N_{\mathrm{Ia}}/(\mathrm{yr}\ \mathrm{Mpc}^3\ h_{70}^{-3})]$
$0.2 \leq \bar{z} < 0.6$	$0.53^{+0.39}_{-0.17}$
$0.6 \leq \bar{z} < 1.0$	$0.93^{+0.25}_{-0.25}$
$1.0 \leq \bar{z} < 1.4$	$0.75^{+0.35}_{-0.30}$
$1.4 \leq \bar{z} < 1.7$	$0.12^{+0.58}_{-0.12}$

Note.—The errors are a quadratic combination of the errors on the d_j^m values listed in Table 11, as well as statistical and systematic errors on the right-hand side of eq. (23).
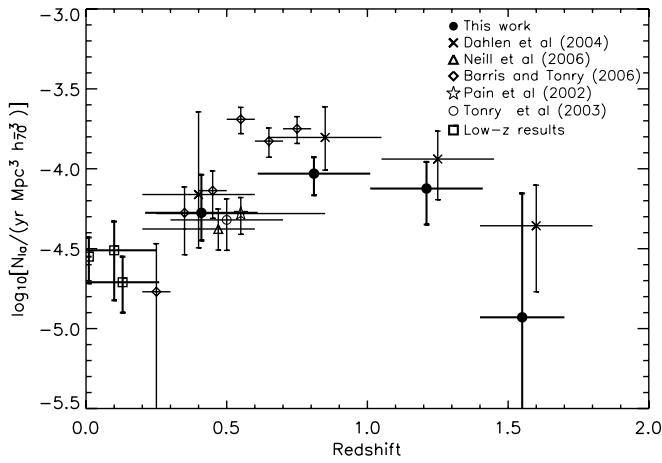
FIG. 6.—*Filled circles*: Results of this work. The first three open squares at low redshifts (the "low-*z* results") are, from lower to higher redshifts, the results of Cappellaro et al. (1999), Madgwick et al. (2003), and Blanc et al. (2004), respectively. The open triangle at $z = 0.47$ is from Neill et al. (2006). The open circle at $z = 0.50$ is from Tonry et al. (2003). The open star at $z = 0.55$ is from Pain et al. (2002). The open diamonds are the results of Barris & Tonry (2006). The crosses are from Dahlen et al. (2004) (including systematic errors). The horizontal bars are estimated redshift bin sizes.

through either the candidate counting or the calculation of the control time/efficiency:

1. *Candidate counting.*—In some bins, the final count of the candidates ends up being about the same for both analyses, but the actual candidates are not the same. This is not unexpected because the techniques used for the SN identification in the two analyses are quite different. Our method provides a probabilistic rather than an absolute identification of each individual SN based on its photometric measurements alone; the same probabilistic approach is used for calculating the efficiency and misidentification. For example, in the highest redshift bin, we have one candidate, but this is from sample 2, which was taken after the work of Dahlen et al. (2004) was published. However, the two high-redshift Type Ia candidates from samples 3 and 4, SN 2002fx and SN 2003ak, that were used in Dahlen et al. (2004) did not pass our stage 2 cuts.

2. *Control time/efficiency.*—A rigorous comparison of the control times is difficult due to the lack of tabulated control time data in Dahlen et al. (2004). However, a rough estimation of the

control time times efficiency factor from the data given in Dahlen et al. (2004) shows that this factor is approximately half our values for all but the highest redshift bin.

6. THE STAR FORMATION HISTORY CONNECTION

A particularly interesting aspect of an SN Ia rates analysis is the possibility of constraining the delay time between the formation of a progenitor star and an SN explosion, which in turn helps constrain possible models for the SN Ia formation. There are two leading models that have been considered in the recent literature: the so-called two-component model and a Gaussian delay model. We now consider both of these models. Unlike in § 4.3, now that we are considering the rates, we can add the low-redshift measurements of Cappellaro et al. (1999), Madgwick et al. (2003), and Blanc et al. (2004) to our results and use the combined data in the fits.

The two-component model (Scannapieco & Bildstren 2005; Mannucci et al. 2006) suggests that the delay function may be bimodal, with one component responsible for the "prompt" SNe Ia that explode soon after the formation of their progenitors and the other for the "tardy" SNe that have a much longer delay time. Following this model, the SN Ia rate can be represented as

$$r_{V,\mathrm{Ia}}(\bar{z}) = A\rho_*(\bar{z}) + B\dot{\rho}_*(\bar{z}), \qquad (26)$$

where $\rho_*(\bar{z})$ is the integrated SFH and $\dot{\rho}_*(\bar{z})$ is the instantaneous SFH. The first term of the equation accounts for the tardy population, while the second term accounts for the prompt one. We use the parametric form of the SFH as given in Hopkins & Beacom (2006):

$$\dot{\rho}_*(\bar{z}) = \frac{(a + b\bar{z})h_{70}}{1 + (\bar{z}/c)^d}, \qquad (27)$$

where $h_{70} = 0.7$, $a = 0.017$, $b = 0.13$, $c = 3.3$, and $d = 5.3$.

The Levenberg-Marquardt least-squares fit of the combined data to the two-component model is shown in the left panel of Figure 7. We obtain $A = (1.5 \pm 0.7) \times 10^{-14}$ yr^{-1} $M_\odot^{-1}$ and $B = (5.4 \pm 2.0) \times 10^{-4}$ yr^{-1} $(M_\odot$ yr$^{-1})^{-1}$. These results are entirely consistent with those obtained by Neill et al. (2006): $A = (1.4 \pm 1.0) \times 10^{-14}$ yr^{-1} $M_\odot^{-1}$ and $B = (8.0 \pm 2.6) \times 10^{-4}$ yr^{-1} $(M_\odot$ yr$^{-1})^{-1}$. The χ^2 of the fit is 5.4 for 5 degrees of freedom.
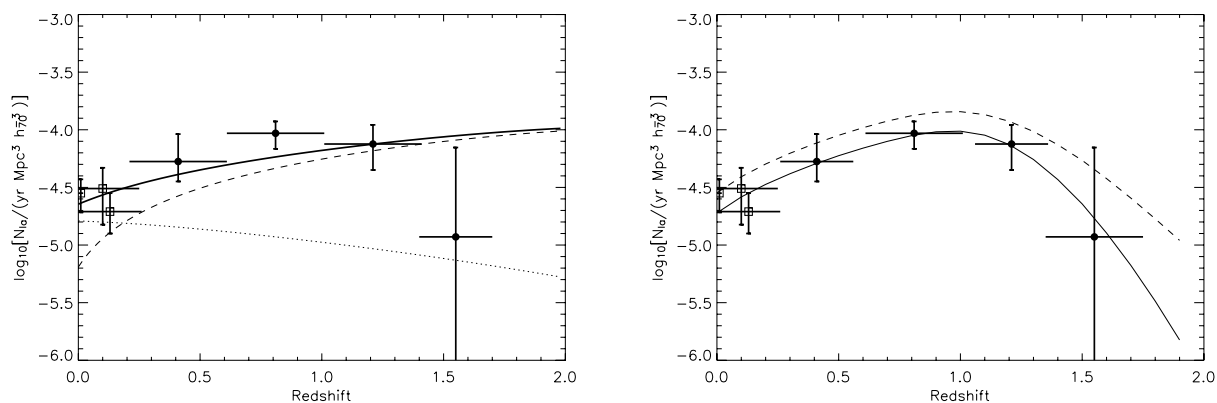

FIG. 7.—*Left*: Least-squares fit of the two-component model to the data. The dashed line represents the prompt component that is proportional to the instantaneous SFH. The dotted line represents the tardy component that is proportional to the integrated SFH. The thick solid line is the sum of the two. *Right*: Gaussian time delay model with our best-fitted parameters (*solid line*), as well as with the parameters of Strolger et al. (2004) (*dashed line*). In both plots, the first three open squares at low redshifts are, from lower to higher redshifts, the results of Cappellaro et al. (1999), Madgwick et al. (2003), and Blanc et al. (2004), respectively. The filled circles are the results of this work. The horizontal bars are estimated redshift bin sizes.

Note that the results of Barris & Tonry (2006) at $z = 0.55$, 0.65, and 0.75 are somewhat inconsistent with our best-fitting two-component model, with the discrepancy at the level of 4.1, 3.2, and 5.2 σ, respectively. This can be seen from Figure 6. It has been argued in Neill et al. (2006) (who also noted that the results of Barris & Tonry [2006] beyond the redshift of 0.5 appear to be rather high) that contamination by non–Type Ia SNe is the most likely source of the problem.

It was suggested in Dahlen et al. (2004) and Strolger et al. (2004) that the SN Ia rate is a convolution of the SFH and a Gaussian time delay distribution function with a characteristic time delay $\tau \sim 3$ Gyr and a $\sigma = 0.2\tau$. Using the Hopkins-Beacom SFH, we find that the best-fitting parameters for such a model are $\tau = 3.2 \pm 0.6$ Gyr and $\sigma = (0.12 \pm 0.54)\tau$, with a fit χ^2 of 2.1 for 4 degrees of freedom. The fit is shown in the right panel of Figure 7. For comparison, we also show the rate model obtained using the parameters from Strolger et al. (2004) ($\tau = 3$ Gyr and $\sigma = 0.2\tau$).

One of the main differences between the two-component model and the time delay model is the predicted behavior at high redshifts: the former predicts an increase in the rates, while the latter, a decrease. From Figure 7 and the results of the fits of our data to both models, we find that neither scenario can be ruled out.

7. SUMMARY

We have analyzed the rates of SNe Ia up to a redshift of 1.7 using two samples collected with the *HST*: the GOODS data and the 2004 ACS sample collected in the spring and summer of 2004 covering the GOODS-N field. Using only the data from two broadband filters, F775W and F850LP, we applied a novel technique for identifying SNe Ia based on a Bayesian probability approach. This method allows us to automatically type SN candidates in large samples, properly taking into account all known sources of systematic error. We also make use of the best currently available full spectral templates for five different SN types for the candidate typing, as well as for calculating the efficiency of our SN search and the control time. These templates will undoubtedly be improved over the next several years as more SN data become available. Current and upcoming SN surveys will not only provide a better understanding of individual SN types, but may also uncover new types of SNe, which can then be added to the Bayesian classification framework. Likewise, a better understanding of the many parameters that affect SN observations will improve the classification scheme, which will result in better constraints on the measured rates. The calculations of the SN finding efficiency, the control time, and the survey area are all done taking into account the specific observing configurations pertinent for the surveys, such as exposure times, cadences, and the orientations of the GOODS tiles.

We carried out a comparison of the predicted and observed numbers of SNe in redshift bins of $\Delta \bar{z} = 0.1$, for two different models of the SN Ia rates: a redshift-independent rate and a power-law redshift-dependent rate. We find that the available data fit both models equally well.

For comparison with previous work, particularly that of Dahlen et al. (2004), who also analyzed a large subset of the data used here, we calculated the volumetric SN Ia rates in four redshift bins, $0.2 \leq \bar{z} < 0.6$, $0.6 \leq \bar{z} < 1.0$, $1.0 \leq \bar{z} < 1.4$, and $1.4 \leq \bar{z} < 1.7$. We find that our results are generally consistent with those of Dahlen et al. (2004). Due to the larger number of SN candidates that this Bayesian classification technique makes available, we obtain smaller or equal uncertainties in all the bins up to $z = 1.7$. In the highest redshift bin we obtain a larger uncertainty because the S/N is generally too low to apply this technique.

We fitted the resulting rates to two leading models used in recent literature: the two-component model and a Gaussian time delay model. The former model implies an increase in the SN Ia rates at highest redshifts, while the latter, a decrease. We find that the statistics of the present sample does not definitively discriminate between the two scenarios: only one SN in this work and two SNe in Dahlen et al. (2004) contribute to the important highest redshift bin. Significantly larger surveillance time would be required to arrive at a conclusive statement on the trends for the Type Ia rates at high redshifts.

In the future, several ambitious new surveys are planned that will collect photometric data for thousands of SNe in order to improve the constraints on dark energy. Individual spectroscopic follow-up for every SN candidate is likely to be impractical in these surveys. The Bayesian classification method described here has the ability to classify SNe using photometric measurements alone and is a promising technique for these future surveys.

REFERENCES

Aldering, G., et al. 2004, PASP, submitted (astro-ph/0405232)
Alexander, D. M., et al. 2003, AJ, 126, 539
Astier, P, et al. 2006, A&A, 447, 31
Barris, B. J., & Tonry, J. L. 2006, ApJ, 637, 427
Bertin, E., & Arnouts, S. 1996, A&AS, 117, 393
Blanc, G., et al. 2004, A&A, 423, 881
Branch, D., Fisher, A., & Nugent, P. E. 1993, AJ, 106, 2383
Cappellaro, E., Evans, R., & Turatto, M. 1999, A&A, 351, 459
Cardelli, J. A., Clayton, G. C., & Mathis, J. S. 1988, ApJ, 329, L33
Chandrasekhar, S. 1931, ApJ, 74, 81
Cohen, J. G., et al. 2000, ApJ, 538, 29
Cowie, L. L., et al. 2004, AJ, 127, 3137
Dahlen, T., & Fransson, C. 1999, A&A, 350, 349
Dahlen, T., et al. 2004, ApJ, 613, 189
Dickinson, M., et al. 2003, in The Mass of Galaxies at Low and High Redshift, ed. R. Bender & A. Renzini (Berlin: Springer), 324
Filippenko, A. V., et al. 1992, AJ, 104, 1543
Fruchter, A., & Hook, R. N. 2002, PASP, 114, 144
Giavalisco, M., et al. 2004, ApJ, 600, L93

Hardin, D., et al. 2000, A&A, 362, 419
Hatano, K., Branch, D., & Deaton, J. 1998, ApJ, 502, 177
Hopkins, A. M., & Beacom, J. F. 2006, ApJ, 651, 142
Hornschemeier, A. E., et al. 2003, AJ, 126, 575
Johnson, B. D., & Crotts, A. P. S. 2006, AJ, 132, 756
Kashikawa, N., et al. 2002, PASJ, 54, 819
Krist, J., & Hook, R. 2004, The Tiny Tim User's Guide (Baltimore: STScI)
Kuznetsova, N., & Connolly, B. M. 2007, ApJ, 659, 530
Le Fèvre, O., et al. 2004, A&A, 428, 1043
Madgwick, D. S., et al. 2003, ApJ, 599, L33
Mannucci, F., Della Valle, M., & Panagia, N. 2006, MNRAS, 370, 773
Neill, J. D, et al. 2006, AJ, 132, 1126
Pain, R., et al. 1996, ApJ, 473, 356
———. 2002, ApJ, 577, 120
Perlmutter, S., & Schmidt, B. P. 2003, in Supernovae and Gamma Ray Bursts, ed. K. Weiler (Berlin: Springer), 598
Perlmutter, S., et al. 1997, ApJ, 483, 565
———. 1999, ApJ, 517, 565
Poznanski, D., Maoz, D., & Gal-Yam, A. 2007a, AJ, 134, 1285

Poznanski, D., et al. 2002, PASP, 114, 833
———. 2007b, MNRAS, 382, 1169
Renzini, A., et al. 2003, in The Mass of Galaxies at Low and High Redshift, ed.
    R. Bender & A. Renzini (Berlin: Springer), 332
Richardson, D., et al. 2002, AJ, 123, 745
———. 2006, AJ, 131, 2233
Riello, M, & Patat, F. 2005, MNRAS, 362, 671
Riess, A. G., et al. 1998, AJ, 116, 1009
———. 2004a, ApJ, 600, L163
———. 2004b, ApJ, 607, 665
———. 2007, ApJ, 659, 98

Rosati, P., et al. 2002, ApJ, 566, 667
Scannapieco, E., & Bildstren, L. 2005, ApJ, 629, L85
Strolger, L.-G., et al. 2004, ApJ, 613, 200
Sullivan, M., et al. 2006a, AJ, 131, 960
———. 2006b, ApJ, 648, 868
Tonry, J. L., et al. 2003, ApJ, 594, 1
van Dokkum, P. G. 2001, PASP, 113, 1420
Vanzella, E., et al. 2006, A&A, 454, 423
Wirth, G. D., et al. 2004, AJ, 127, 3121
Wolf, C., et al. 2004, A&A, 421, 913